ORIGINAL RESEARCH

Loss of Apelin Exacerbates Myocardial Infarction Adverse Remodeling and Ischemia-reperfusion Injury: Therapeutic Potential of Synthetic Apelin Analogues

Wang Wang, MSc; Shaun M.K. McKinnie, BSc; Vaibhav B. Patel, PhD; George Haddad, PhD; Zuocheng Wang, PhD; Pavel Zhabyeyev, PhD; Subhash K. Das, MSc; Ratnadeep Basu, MD; Brent McLean, BSc; Vijay Kandalam, PhD; Josef M. Penninger, MD; Zamaneh Kassiri, PhD; John C. Vederas, PhD; Allan G. Murray, MD; Gavin Y. Oudit, MD, PhD, FRCP(C)

Background—Coronary artery disease leading to myocardial ischemia is the most common cause of heart failure. Apelin (APLN), the endogenous peptide ligand of the APJ receptor, has emerged as a novel regulator of the cardiovascular system.

Methods and Results—Here we show a critical role of APLN in myocardial infarction (MI) and ischemia-reperfusion (IR) injury in patients and animal models. Myocardial APLN levels were reduced in patients with ischemic heart failure. Loss of APLN increased MI-related mortality, infarct size, and inflammation with drastic reductions in prosurvival pathways resulting in greater systolic dysfunction and heart failure. APLN deficiency decreased vascular sprouting, impaired sprouting of human endothelial progenitor cells, and compromised in vivo myocardial angiogenesis. Lack of APLN enhanced susceptibility to ischemic injury and compromised functional recovery following ex vivo and in vivo IR injury. We designed and synthesized two novel APLN analogues resistant to angiotensin converting enzyme 2 cleavage and identified one analogue, which mimicked the function of APLN, to be markedly protective against ex vivo and in vivo myocardial IR injury linked to greater activation of survival pathways and promotion of angiogenesis.

Conclusions—APLN is a critical regulator of the myocardial response to infarction and ischemia and pharmacologically targeting this pathway is feasible and represents a new class of potential therapeutic agents. **(*J Am Heart Assoc.* 2013;2: e000249 doi: 10.1161/JAHA.113.000249)**

Key Words: angiogenesis • cardiomyopathy • heart failure • ischemia-reperfusion injury • myocardial infarction

Apelin (APLN) is the endogenous ligand for the apelin receptor (APJ receptor) and is synthesized as a 77-amino acid prepropeptide which is processed into C-terminal fragments denoted by their lengths as Apelin-36, Apelin-19, Apelin-17 and Apelin-13.[1,2] APLN is predominantly expressed in the endocardial and vascular endothelial cells while the APJ receptor is localized to endothelial and smooth muscle cells as well as cardiomyocytes, allowing for autocrine and paracrine effects of APLN in the heart.[2–4] APLN mediates positive inotropic effect on isolated cardiomyocytes,[5] isolated perfused rat heart[6] and in vivo[7] and mediates endothelium-dependent vasodilation.[8] Genetic variation in the APJ receptor modifies the progression of heart failure in patients with dilated cardiomyopathy[9] and the APLN /APJ system is compromised in human heart failure.[3,10] In patients with chronic heart failure, APLN administration increased cardiac index and lowered peripheral vascular resistance in the absence of hypotension providing a promising new drug target for heart failure.[11]

Coronary artery disease is now the most common cause of heart failure.[12] APLN promotes the phosphorylation of Akt and increases the proliferation of endothelial cells in vitro suggesting an important proangiogenic role.[13–15] Given the

From the Departments of Physiology (W.W., R.B., B.M., V.K., Z.K., G.Y.O.) and Chemistry (S.M.K.M., J.C.V.); Mazankowski Alberta Heart Institute (W.W., V.B.P., Z.W., P.Z., S.K.D., R.B., B.M., V.K., Z.K., G.Y.O.); Divisions of Cardiology (V.B.P., Z.W., P.Z., S.K.D., G.Y.O.) and Nephrology (G.H., A.G.M.), Department of Medicine, University of Alberta, Edmonton, Alberta, Canada; Institute of Molecular Biotechnology of the Austrian Academy of Sciences, Vienna, Austria (J.M.P.).

Accompanying Tables S1 through S3 and Figures S1 through S12 are available at http://jaha.ahajournals.org/content/2/4/e000249/suppl/DC1.

Correspondence to: Gavin Y. Oudit, MD, PhD, FRCP(C), Division of Cardiology, Department of Medicine, Mazankowski Alberta Heart Institute, University of Alberta, Edmonton, Alberta, T6G 2S2, Canada. E-mail: gavin.oudit@ualberta.ca.

Received April 6, 2013; accepted June 5, 2013.

plethora of biochemical and cellular effects of APLN, we hypothesized that loss of APLN may enhance the susceptibility to myocardial ischemic injury. We used APLN knockout ($APLN^{-/y}$) and wildtype ($APLN^{+/y}$) mice and showed that loss of APLN impaired the functional recovery, post-MI remodeling and angiogenesis and exacerbate myocardial ischemia-reperfusion (IR) injury. We used novel synthetic APLN analogues, which were markedly more resistant to proteolytic cleavage by angiotensin converting enzyme 2 (ACE2) than native pyr-1-apelin-13, and identified one analogue that mimicked the function of APLN and resulted in marked protection against ex vivo and in vivo myocardial IR injury. We conclude that APLN critical regulates the myocardial response to ischemia and pharmacologically targeting this pathway is feasible and represents a new class of potential therapeutic agents.

Methods

Experimental Animals

APLN -deficient ($APLN^{-/y}$) and littermate wildtype ($APLN^{+/y}$) mice were generated and bred in a C57BL/6 background as previously described.[16] All animal experiments were carried out in accordance with the Canadian Council on Animal Care Guidelines, and animal protocols were reviewed and approved by the Animal Care and Use Committee at the University of Alberta.

Human Explanted Hearts

Cardiac tissues from patients with subacute MI or idiopathic dilated cardiomyopathy and with advanced heart failure were collected from the explanted hearts at the time of cardiac transplantation as part of the Human Explanted Heart Program (HELP) at the Mazankowski Alberta Heart Institute. Nonfailing control hearts were obtained by the Human Organ Procurement and Exchange (HOPE) program. All experiments were performed in accordance with the institutional guidelines and were approved by Institutional Ethics Committee.

Myocardial Infarction

Ten-week-old male mice of both genotypes were subjected to MI by permanent ligation of the proximal left anterior descending (LAD) coronary artery in a manner blinded to the genotype as previously described.[17,18] Anaesthetized mice underwent left thoracotomy in the fourth intercostal space. The pericardium was opened to expose the left ventricle (LV) and the LAD was encircled and ligated with a 6-0 silk suture; the muscle and skin were closed in layers. In sham-operated mice, LAD was encircled but not ligated. Animals were inspected at least 2 times daily. Following 1 day, 3 days, and 7 days after LAD ligation or sham-operation, mice were anaesthetized and sacrificed. Hearts were quickly excised, dissected into infarct, peri-infarct, and noninfarct regions, and then flash-frozen separately for further protein and RNA analyses. For immunohistochemical analysis, whole hearts were arrested in diastole with 1 mol/L KCl and then fixed in 10% formalin or embedded in optimal cutting temperature compound (OCT) and flash frozen.

Infarct Size Measurement and Neutrophil and Macrophage Staining

For infarct size measurement, hearts were quickly excised and sectioned in 0.5-mm slices from apex to the point of ligation, then incubating with 1% Triphenyl Tetrazolium Chloride at 37°C for 10 minutes. The brick red represents viable tissue, while pale indicates necrosis. Image Proplus software was used for image analysis. Infarct size was reported as a percentage of the total LV size. Neutrophils and macrophages were stained in sham, 1-day and 3-days post-MI LVs using rat antimouse neutrophil (AbD Serotec) and rat antimouse Mac-3 (BD Biosciences) primary antibodies and Cy3 conjugated goat antirat and Alexa Fluor 488 conjugated goat antirabbit secondary antibodies (Invitrogen), respectively. The sections were visualized and imaged under fluorescence microscope (Olympus IX81) and images were analyzed using Metamorph software (Version 7.7.0.0).

APLN and CD31 Immunofluorescence

APLN and CD31 double immunofluorescence staining was carried out in human heart and coronary arteries as well as in murine heart tissues. Briefly, 5 μm thick OCT embedded cryosections were fixed with 4% paraformaldyhyde followed by rehydration, permeabilization and blocking with PBS, 0.1% triton X-100 and 4% BSA, respectively. The sections were then incubated with primary antibodies, goat anti-APLN (Santa Cruz Biotechnology Inc.) and mouse antihuman CD31 (BD Biosciences) for human LV and goat anti- APLN (Santa Cruz Biotechnology Inc.) and rat antimouse CD31 (BD Biosciences), at 4°C for overnight. The sections were then washed with PBS and incubated with secondary antibodies, Alexa Fluor 488 conjugated donkey antigoat and Alexa Fluor 594 conjugated donkey antimouse for human LV and Alexa Fluor 488 conjugated donkey antigoat and Alexa Fluor 594 conjugated donkey antirat (Invitrogen) for mouse LV, at 37°C for 1 hour. The sections were washed with PBS, mounted with Prolong Gold antifade mounting medium with DAPI (Invitrogen) and visualized and imaged under the fluorescence microscope (Olympus IX81).

Echocardiography Measurements and Invasive Pressure-Volume Analysis

Transthoracic echocardiography was performed noninvasively as described previously using a Vevo 770 high-resolution imaging system equipped with a 30-MHz transducer (RMV-707B; VisualSonics). The temporal resolution for M-mode imaging in this system is a pulse repetition frequency of 8 kHz with an axial resolution of 55 μm, lateral resolution of 115 μm, focal length of 12.7 mm, and depth of field of 2.2 mm. Mice were anesthetized with 0.8% isoflurane for the duration of the recordings. LV ejection fraction (EF) was calculated as a measure of systolic function using the following equation: EF (%)=([LV end-diastolic volume−LV end-systolic volume]/LV end-diastolic volume)/100. The maximal anteroposterior left atrial (LA) diameter was measured by M-mode in the parasternal long-axis view and used as LA size. Qualitative and quantitative measurements were made offline using analytic software (VisualSonics). Electrocardiogram kilohertz-based visualization (EKV™) software analysis produced offline reconstruction for simulated 250 to 1000 Hz static and cine loop images. Modified parasternal long axis EKV loops were also used to measure EF via Simpson's method. M-mode images were used to measure LV chamber sizes and wall thicknesses. The wall motion score index (WMSI) was calculated based on the *American Society of Echocardiography* recommended assessment of wall motion function of the 17-segment LV model.[19–21] In the murine model, use of WMSI and analysis of segmental wall motion abnormalities in the post-MI hearts has been validated.[19,20]

To measure LV pressure-volume relationship, 1.2F admittance catheter (Scisense Inc.) was used as previously described.[22,23] Briefly, mice were anaesthetized with isoflurane; an incision was made in the right carotid artery and a catheter was inserted into the incision. The catheter was advanced to the LV via ascending aorta and aortic valve. The position of the catheter was monitored by pressure along with the magnitude and phase using ADvantage pressure-volume system (Scisense Inc.) and iworx (iWorx Systems Inc.) data acquisition system connected to the catheter. Initially, the catheter position was set in the LV to obtain the magnitude difference of more than 200 μS along with a physiological pressure-volume loop shape. After the magnitude was accomplished in the desired range, the phase was adjusted to 4 to 8 with slightly adjusting the position of the catheter in the LV where phase represents the conductivity imparted by the LV tissue. Once, the desired range for magnitude and phase was achieved, a baseline scan was performed to derive volume using Baan's equation and pressure-volume loop was obtained using the LabScribe2 software (version 2.347000). After the instrument (ADvantage, Scisense Inc.) was adjusted and PV measurements were obtained, the inferior vena cava was briefly occluded to obtain alterations in venous returns to derive end-systolic and end-diastolic PV relations. Online as well as offline calculations were performed using LabScribe2 software (version 2.347000).

Synthesis and Characterization of Novel APLN Analogues

Reagents and solvents

All commercially available reagents and protected amino acids were purchased and used without further purification. Dichloromethane (DCM) used for anhydrous reaction was distilled over calcium hydride prior to use. High-performance liquid chromatography (HPLC) grade dimethylformamide (DMF) and methanol were used without further purification.

Loading of C-terminal 4-bromophenylalanine onto Wang resin

A flame dried 3-necked round bottom flask equipped with a stirring bar was flushed with Ar gas. Fmoc-4-bromophenylalanine (0.933 g, 2.0 mmol) was dissolved in dried DCM and cooled to 0°C. Diisopropylcarbodiimide (0.155 mL, 1.0 mmol) was added to the mixture and stirred at 0°C for 20 minutes. The reaction mixture was concentrated in vacuo and redissolved in a DMF:DCM solution (3:1). Wang resin (2.00 g) was added to a solid phase peptide synthesis vessel and washed with dry DCM (2×10 mL) and DMF (2×10 mL). The resin was preswollen by bubbling with Ar gas in DMF (10 mL) for 1 hour and filtered. The activated Fmoc-4-bromophenylalanine anhydride was added to the resin followed by catalytic 4-dimethylaminopyridine (DMAP) and bubbled under Ar gas for 1.5 hours. The solution was drained, and the resin was washed with DMF (3×10 mL). To cap additional reactive sites on the resin, 20% acetic anhydride in DMF (15 mL, 15 minutes) was used and followed by washing with DMF (3×10 mL) and DCM (3×10 mL), yielding Fmoc-4-bromophenylalanine on Wang resin in 0.5 mmol/g loading.

General procedure for elongation using manual Fmoc Solid Phase Peptide Synthesis

N-methylmorpholine (NMM) (6 equiv) was added to a solution of Fmoc protected amino acid (5.0 equiv to resin loading), 1-hydroxybenzotriazole hydrate (HOBt) (5.0 equiv) and benzotriazol-1-yl-oxytripyrrolidinophosphonium hexafluorophosphate (PyBOP) (4.9 equiv) in DMF (10 mL). The solution was allowed to preactivate for 5 minutes. The solution was transferred to the reaction vessel containing preswelled resin and was bubbled with argon for 2 hours. A small sample of the peptide was cleaved from the resin (by treatment with 95% trifluoroacetic acid (TFA)/2.5% triisopropylsilane (TIPS)/2.5% water (H_2O) for 2 hours) and the completion of the reaction

was determined by matrix-assisted laser desorption/ionization – time of flight (MALDI-TOF) analysis using 4-hydroxy-α-cyanocinnamic acid (HCCA) as a matrix. Resin was washed with DMF (3×10 mL), then 20% Ac_2O in DMF (10 mL) was added to the resin for 10 minutes to affect end capping. Resin was again washed with DMF (3×10 mL). Then 20% piperidine in DMF (3×10 mL) was added to remove the N-terminal Fmoc protecting group, this reaction was monitored by ultraviolet-visible (UV-Vis) spectroscopy, observing the dibenzofulvene-piperidine adduct at λ=301 nm.

General procedure for peptide synthesis using automated Fmoc Solid Phase Peptide Synthesis

All peptides were synthesized on a CEM Liberty 1 Microwave Peptide Synthesizer. Solid phase synthesis was carried out on a 0.1 mmol scale using Fmoc chemistry on Wang resin (0.65 mmol/g loading). Commercially available protected amino acids and were loaded on the peptide synthesizer as 0.2 mol/L solutions in DMF. All amino acid subunits were coupled using O-benzotriazole-N,N,N',N'-tetramethyl-uronium-hexafluoro-phosphate (HBTU) as the activating agent and heated at 70°C for a 5 minutes coupling time. Fmoc residues were deprotected using a 20% solution of piperidine in DMF using UV-Vis spectroscopy to observe the dibenzofulvene-piperidine adduct absorption monitored at λ=301 nm.

Syntheses of NleInpBrF pyr-1-apelin-13 and NleAibBrF pyr-1-apelin-13 analogues

For both analogues, 4-bromophenylalanine-loaded Wang resin was subjected to Fmoc deprotection as described above, and either Fmoc-Inp-OH or Fmoc-Aib-OH were coupled onto the free amine to initiate the synthesis of NleInpBrF or NleAibBrF pyr-1-apelin-13, respectively. The following amino acids were coupled as previously described in the following order: Fmoc-Nle-OH, Fmoc-Pro-OH, Fmoc-Gly-OH, Fmoc-Lys(Boc)-OH, Fmoc-His(Trt)-OH, Fmoc-Ser(O^{t}Bu)-OH, Fmoc-Leu-OH, Fmoc-Arg(Pmc)-OH, Fmoc-Pro-OH, Fmoc-Arg(Pmc)-OH, and pyroglutamic acid.

General procedure for cleavage and purification of pyr-1-apelin-13 analogues

To simultaneously cleave the peptide from Wang resin and remove side chain protecting groups, a solution of 95:2.5:2.5 TFA:anisole:H_2O was added to the resin-bound peptide for 2 hours. The resin beads were removed via filtration through glass wool and the filtrate was concentrated in vacuo. The crude peptide was obtained by precipitation with cold Et_2O. The crude peptide was redissolved in a 9:1 H_2O:methanol (0.1% TFA) solution and purified by HPLC, which was performed on a Varian Prostar chromatograph equipped with a model 325 variable wavelength UV detector and a Rheodyne 7725i injector fitted with a 1000 μL sample loop. The column used for semipreparative purification was a Phenomenex Luna C18(2) column (5 μm, 10.00×250 mm), and for analytical purification was a C18 reverse-phase peptide/protein HPLC column (Vydac, 4.6×250 mm, 5 μm) using H_2O (0.1% TFA) and acetonitrile (0.1% TFA) as eluents. All HPLC solvents were filtered with a Millipore filtration system under vacuum before use.

The HPLC method followed was: gradient beginning at 2% acetonitrile, climb to 50% acetonitrile over 10 minutes, then climb to 100% acetonitrile over 4 minutes, remain at 100% for 4 minutes, return to 2% over 4 minutes, hold at 2% over 3 minutes (flow rate 1 mL/min [analytical] or 2.5 mL/min [semipreparative] with UV detection at 220 nm). The peptide was collected as a sharp peak at 13.5 minutes and solvent was removed in vacuo. The residue was then resuspended in 0.1% TFA in H_2O and lyophilized to give the final product. NleInpBrF pyr-1-apelin-13 (apelin analogue I) was isolated as a white solid powder after lyophilization in 25.6% yield (10.5 mg purified). NleAibBrF pyr-1-apelin-13 (apelin analogue II) was isolated as a white solid powder after lyophilization in 36.4% yield (17.9 mg purified).

Angiotensin-converting Enzyme 2 Proteolysis Assay of pyr-1-apelin-13 and APLN Analogues

Recombinant angiotensin converting enzyme 2 (rACE2) was suspended in Tris buffer (25 mmol/L Tris, 200 mmol/L NaCl, 5 μmol/L $ZnCl_2$, pH 8.0) to a final concentration of 1 μmol/L. 1 mmol/L solutions of APLN peptides (pyr-1-apelin-12 [65 to 76] [New England Peptide Inc] and pyr-1-apelin-13 [65 to 77] [Tocris Bioscience]) and APLN analogues were prepared in Milli-Q water. A modified procedure was adapted to determine the extent of susceptibility of APLN peptides and APLN analogues to ACE2 proteolysis.[24] 5 μL of 1 μmol/L recombinant ACE2 was added to 90 μL of buffer (25 mmol/L Tris, 200 mmol/L NaCl, 5 μmol/L $ZnCl_2$, pH 8.0) and 5 μL of aqueous 1 mmol/L APLN peptide or APLN analogue were added to the reaction mixture for varying quantities of time at room temperature or 37°C to achieve final concentrations of 5 nmol/L rACE2 and 5 μmol/L APLN peptide/analogue, respectively. Reactions were quenched upon addition of 100 μL of 100 mmol/L ethylenediaminetetraacetic acid (EDTA) pH 7.0, and products were monitored by both HPLC and MALDI-TOF analyses. Analytical HPLC separation of peptides was accomplished using a C18 reverse-phase peptide/protein HPLC column (Vydac, 4.6×250 mm, 5 μm) using a gradient of 10% to 45% B (A: H_2O [0.1% TFA]; B: acetonitrile [0.1% TFA]). A flow rate of 1 mL/min was used and peptides were detected by absorbance at 220 nm. The

amount of hydrolyzed product was determined by comparing the areas under the substrate and product peaks after integration as previously reported.[24] Hydrolysis products and initial substrates were analyzed on a Perspective Biosystems Voyager™ Elite MALDI-TOF MS using 4-hydroxy-α-cyanocinnamic acid (HCCA) as a matrix to confirm masses.

Isolated Langendorff Heart Perfusion and Ischemia-Reperfusion Protocol

Langendorff heart perfusion was used to study the contractile function. Mice were heparinized and anaesthetized with 1.5% to 2% isoflurane inhalation. Heart was excised and mounted on Langendorff system and perfused at a consistent pressure of 80 mm Hg with modified Krebs-Henseleit solution (116 mmol/L NaCl, 3.2 mmol/L KCl, 2.0 mmol/L $CaCl_2$, 1.2 mmol/L $MgSO_4$, 25 mmol/L $NaHCO_3$, 1.2 mmol/L KH_2PO_4, 11 mmol/L glucose, 0.5 mmol/L EDTA and 2 mmol/L pyruvate), which was kept at 37°C and continuously oxygenated with 95% O_2 and 5% CO_2 to maintain a pH at 7.4. By inserting a water-filled balloon into the LV chamber, which on the other side connected to a pressure transducer, the pressure changes were recorded by PowerLab system (ADInstruments). After stabilization and 10 minutes baseline recording, global ischemia was induced for 30 minutes followed by 40 minutes of reperfusion and hearts were flash frozen in liquid nitrogen. The coronary effluents were collected at baseline, at the start of reperfusion, and following 10 minutes of reperfusion, for the determination of CK activity. A postconditioning protocol with wildtype ($APLN^{+/y}$) hearts was used with APLN analogue I and II (1.5 μg/mL for 20 minutes) given at the start of reperfusion.

Myocardial Ischemia-Reperfusion Injury In-Vivo

Ten-week-old male mice of both genotypes were subjected to ischemia by LAD ligation followed by reperfusion. Reliability of IR was confirmed by Evan's blue staining. Anaesthetized mice underwent left thoracotomy in the fourth intercostal space. The pericardium was opened to expose the LV and the LAD coronary artery was encircled and ligated with a 6-0 silk suture for 30 minutes; the reperfusion was established by releasing the ligation. In sham-operated mice, the LAD was encircled but not ligated. Following 3 hours of reperfusion or sham-operation, mice were reanaesthetized and sacrificed. The non-IR parts of the hearts were distinguished with Evan's Blue by injection into the coronary circulation after the LAD was ligated again at the same location. Hearts were quickly excised and sectioned in 1-mm slices from apex to the point of ligation, then incubating with 1% triphenyl tetrazolium chloride (TTC) (Sigma) at 37°C for 10 minutes. The blue stained area represents the non-IR myocardium while the rest was termed area at risk (AAR) in which the brick red represents viable tissue, while the white/yellowish region indicates nonviable tissue. In a separate group of wildtype mice, APLN analogue II (60 μg/kg/min for 10 minutes) was administered via the right internal jugular vein at the moment of reperfusion.

CK Activity Assay

Perfusates from the Langendorff preparations and plasma from 1-day post-MI mice were collected and preserved at −80°C for creatine kinase (CK) activity assay using a commercial kit (BioAssay).

Aortic Ring Angiogenesis Assay

The ex vivo mouse ring angiogenesis assay was carried as previously described.[25] Thoracic aorta excised from 10-week old $APLN^{+/y}$ and $APLN^{-/y}$ mice under sterile conditions were cut into 1 mm-thick rings under a stereomicroscope. The aortic rings were placed between two layers of Matrigel matrix (BD Biosciences; 354234) in a 48-well culture plate. EBM-2 media (Lonza; CC-3156) with 2% FBS was added containing PBS, rhVEGF (20 ng/mL; Lonza; CC-4114A), APLN analogue I and II (100 ng/mL). Rings were cultured at 37°C and 5% CO_2 for 12 days. Phase-contrast images were taken using an Olympus IX81 microscope.

Fibrin Gel Bead Angiogenesis Assay

Human endothelial progenitor cells (hEPCs) were isolated from peripheral blood as previously described.[26] Briefly, mononuclear blood cells were isolated from leukopheresis products under a protocol approved by the Health Ethics Review Board of the University of Alberta. After density separation over a ficol gradient, CD34+ cells were isolated using antibody-coated magnetic beads (StemCell Technologies). The late outgrowth endothelial colony-forming cells (ECFC) clones were expanded in EBM-2 medium with 10% FBS, and routinely monitored for expression of endothelial marker gene products using quantitative RT-PCR, flow cytometry, or Western blot. Where indicated, hEPCs were transfected with 50 mmol/L non-silencing or siRNA directed to APLN (Qiagen) and in vitro angiogenesis of hEPCs was evaluated as described previously.[27,28] EPCs transfected with si Nonsense (siNS) or siAPLN were loaded onto Cytodex (Sigma) beads (~400 cells/bead) and cultured for 2 hours, then the beads were suspended in fibrinogen/fibronectin solution (2 mg/mL) containing aprotinin (0.15 U/mL) and 0.625 U/mL thrombin was added. Images of the beads after 16 hours culture were captured using a 20× objective and a charge-coupled device (CCD) camera-equipped inverted microscope (Leica). The

number and length of sprouts were analyzed using image analysis software (OpenLab) of 30 beads/experiment. Sprout length was grouped into tertiles established from mock-transfected hEPC (<75, 76 to 125, >126 μm).

Isolated Cardiomyocyte Contractility

Adult murine LV cardiomyocytes were isolated and cultured as previously described except that the 2,3-butanedione monoxime was omitted to preserve contractile function.[29–31] Briefly, mice were injected with 0.05 mL of 1000 USP/mL heparin for 15 minutes and then anesthetised using 2% isoflurane (1 L/min oxygen flow rate) provided through a nose cone. After opening the chest cavity, the heart was quickly excised and perfused using a Langendorff system within 45 s. Following 3-minute perfusion, the heart was then digested with 2.4 mg/mL collagenase type 2 (Worthington) for 7 to 8 minutes. After sufficient digestion, the ventricles were removed, dissociated using forceps and transfer pipettes, and resuspended in stopping buffer (10% FBS perfusion buffer). The isolated cardiomyocytes were then exposed to increasing Ca^{2+} concentrations (100 μmol/L, 400 μmol/L, and 900 μmol/L) for 15 minutes each and were kept in perfusion buffer solution (pH 7.4). An aliquot of isolated cardiac myocytes were transferred in a glass-bottomed recording chamber on top of inverted microscope (Olympus IX71) and allowed to settle for 5 to 6 minutes. Cells were superfused at a rate of 1.5 to 2 mL/min with modified Tyrode's solution (containing in mmol/L: 135 NaCl, 5.4 KCl, 1.2 $CaCl_2$, 1 $MgCl_2$, 1 NaH_2PO_4, 10 taurine, 10 HEPES, 10 glucose; pH 7.4 with NaOH). The perfusion solutions were heated to an in-bath temperature of 35 to 36°C using in-line heater (SH-27B, Harvard Apparatus) controlled by automatic temperature controller (TC-324B, Harvard Apparatus). Quiescent rod–shaped myocytes with clear striations were selected for study. Platinum-wire electrodes were placed near the cell just outside of the microscope view at 400× magnification. Cardiomyocytes were paced at 1 Hz with voltage of 3 to 4 V (50% above threshold) and pulse duration of 2.5 ms using S48 stimulator (Grass Technology). Sarcomere length was estimated in real time from images captured at a rate 200 frame/sec via 40× objective (UAPO 40×3/340, Olympus) using high-speed camera (IMPERX IPX-VGA-210, Aurora Scientific). Sarcomere length was calculated by HVSL software v. 1.75 (Aurora Scientific) using auto-correlation function (ACF/Sine-fit) algorithm. Myocytes were paced for at least 2 minutes. Only recordings of myocytes that produced stable contractions at a steady-state were selected for analysis. At about 2 minutes of stimulation time, 10 consecutive contractions were selected and averaged to reduce noise and make calculations of derivatives more precise. Averaged contraction was used to calculate fractional shortening (FS), relaxation times (t50 and t90), and ±dL/dt. Calculations were performed in Origin 8.5 (OriginLab) using custom-made script of built-in LabTalk language.

TUNEL, CD31, Lectin and HIF-1α Immunofluorescence

In situ DNA fragmentation was detected by TUNEL assay kit (Invitrogen) according to manufacturer's instructions. Briefly, 5 μm-thick LV cryosections were fixed with 4% paraformaldehyde and washed in Dulbecco's PBS. The sections were then permeabilized with 0.1% Triton X-100 in 0.1% sodium citrate and washed with wash buffer. After one hour incubation with DNA labeling solution (terminal deoxynucleotidyl transferase and BrdUTP in reaction buffer) the sections were treated with Alexa Fluor 488 conjugated mouse anti-BrdU and counterstained with propidium iodide. The sections were mounted using Prolong Gold antifade mounting medium and visualized under fluorescence microscope (Olympus IX81). Terminal deoxynucleotidyl transferase mediated dUTP nick end labeling (TUNEL) positive cells were counted using 20× magnification images with MetaMorph (Basic version 7.7.0.0) software and magnitude of apoptosis was expressed as a percentage of apoptotic cells.

Vascular endothelial cells were stained in sham and 7 days post-MI LVs by immunohistochemistry using rat anti-CD31 (BD Pharmingen) primary antibody and Cy3 conjugated goat antirat (Invitrogen) secondary antibody. Briefly, 5- μm thick OCT-embedded cryosections were fixed with 4% paraformaldehyde, permeabilized with 0.2% Triton X100, and blocked with 4% bovine serum albumin. The sections were then incubated with primary antibody (1:10, clone MEC 13.3, BD Pharmingen) overnight at 4°C in a humidified chamber. After several washings the sections were incubated with Cy3 conjugated goat antirat (Invitrogen) secondary antibody for 1 hour at 37°C. The sections were visualized and imaged under fluorescence microscope (Olympus IX81) after mounting with Prolong Gold antifade mounting medium (Invitrogen). The images were analyzed using Metamorph software (Version 7.7.0.0) and the magnitude of vascularization was represented as CD31[+] area/mm^2 of the myocardium.

Lectin immunofluoresence assay using fluorescein conjugated *Ricinus communis* agglutinin I (RCA; lectin; Vectorlabs) perfusion method was used to assess blood flow and new vessel formation in peri-infarct area after 7 days of MI or sham surgery in $APLN^{+/y}$ and $APLN^{-/y}$ mice. Briefly, heparinized mice were anesthetized with ketamine (100 mg/kg) and xylazine (10 mg/kg) and right jugular vein was cannulated using PE10 tubing. 0.2 mg of lectin in 100 μL saline was injected into the jugular vein; 50 μL of saline was injected immediately to expel lectin from cannula. After 18 minutes of lectin circulation, 0.2 mg of papaverine HCl (Sigma Aldrich) in

50 μL saline was injected through the same cannula to promote maximal dilation of blood vessels and circulated for 2 minutes. After 20 minutes of lectin administration, hearts were collected in OCT in cold conditions. Five-μm thick cryosections were cut, fixed with 4% paraformaldehyde for 20 minutes followed by rehydration using PBS for 30 minutes. The sections were mounted in Prolong Gold antifade mounting medium with DAPI (Invitrogen), visualized, and imaged under fluorescence microscope (Olympus IX81). Images were analyzed using Metamorph (Version 7.7.0.0) software and magnitude of vascularization in peri-infarct area was represented as lectin perfused area/mm^2 of the myocardium.

To assess the nuclear translocation of hypoxia inducible factor-1α (HIF-1α), a key mediator of cellular adaptation to hypoxia, immunofluorescence was performed on 5-μm thick formalin fixed-paraffin embedded sections. Briefly, after deparaffinization sections were heated to 95 to 100°C in citrate buffer pH 6.0 for the antigen retrieval. The sections were than immune-stained with anti-Hif-1α primary antibody (Novus Biologicals) and TRITC conjugated antirabbit secondary antibody (Invitrogen) and counterstained DAPI. The section were mounted and visualized under fluorescence microscope (Olympus IX81) and nuclear HIF-1α expression in the peri-infarct region was morphometrically measured using Metamorph (Version 7.7.0.0) software.

TaqMan Real-time PCR

RNA expression levels of various genes were determined by TaqMan real-time PCR as previously described (see Table S1 for list of primers and probes).[17,32] Total RNA was extracted from flash-frozen tissues using TRIzol, and cDNA was synthesized from 1 μg RNA by using a random hexamer. For each gene, a standard curve was generated using known concentrations of cDNA (0.625, 1.25, 2.5, 5, 10, and 20 μg) as a function of cycle threshold (CT). Expression analysis of the reported genes was performed by TaqMan real-time-PCR using ABI 7900 Sequence Detection System. The SDS2.2 software (integral to ABI7900 real-time machine) fits the CT values for the experimental samples and generates values for cDNA levels. All samples were run in triplicates in 384 well plates. 18S rRNA was used as an endogenous control.

Western Blot Analysis and Nuclear Fractionation

Total protein extraction and immunoblotting (IB) were performed as previously.[30] Typically, 150 μg of total protein isolated from LV was separated on 8% or 14% sodium dodecyl sulfate polyacrylamide gel electrophoresis (SDS-PAGE) and subject to IB of phospho-(Ser473)/total Akt and phospho/total Erk1/2 (Cell Signaling Technology); and of anti APLN (ab59469) and anti-APJ receptor (ab84296) from Abcam Inc. The anti-APLN antibody (ab59469) was raised against the conserved C-terminus of APLN. VEGF (147) and α-Tubulin (DM1A) antibodies were purchased from Santa Cruz Biotechnology Inc. Blots were visualized and quantified with ImageQuant LAS 4000 (GE Healthcare). Western blot for phospho-(serine-473)/total Akt was also performed on hEPCs. Human EPCs were serum-starved overnight in incomplete EBM-2 supplemented with 2% FBS. The next day EPCs were stimulated with placebo (PBS), APLN analogue I and II at 30 and 100 ng/mL for 10 minutes and cells were collected for analysis of phospho-Akt (Ser473)/total Akt levels.

Nuclear fractionation was performed as previously described[33] with modifications. Briefly, LV tissues were homogenized in hypotonic lysis buffer (10 mmol/L K-HEPES (pH 7.9), 1.5 mmol/L $MgCl_2$, 10 mmol/L KCl, 1 mmol/L DTT, 0.2 mmol/L Na_3VO_4, 1× protease inhibitor cocktail (Calbiochem), 1× phosphatase inhibitors (Sigma and Calbiochem). The total homogenate was centrifuged at 100*g* for 5 minutes to collect unbroken tissues. The supernatant was then centrifuged at 2000*g* for 10 minutes to precipitate crude nuclei from cell membrane and cytosolic proteins (second supernatant). The second supernatant was further centrifuged at 100 000*g* for 90 minutes to separate soluble cytosolic proteins (third supernatant) from membrane pellet. The crude nuclear fraction was resuspended in hypotonic lysis buffer supplemented with 2.4 mmol/L sucrose, and then layered on top of a 2.4 mmol/L sucrose cushion and purified by centrifugation at 100 000*g* for 90 minutes. Following ultracentrifugation, the purified nuclear pellet was resuspended in storage buffer (20 mmol/L Na-HEPES [pH 7.9], 0.42 mol/L NaCl, 1.5 mmol/L $MgCl_2$, 0.2 mmol/L EDTA, 0.2 mmol/L EGTA, 0.5 mmol/L PMSF, 0.5 mmol/L DTT, 25% Glycerol, 1× protease and phosphatase inhibitors). 30 μg of nuclear protein from LV was subject to HIF1α blotting (Novus). The purity of nuclear and cytosolic fractions was verified by using Histone H-3 (Cell Signaling; nuclear marker) and Caspase-3 (Cell Signaling; cytosolic marker).

Statistical Analysis

Statistical analyses were performed using the SPSS Statistics 19 software and statistical significance was recognized at $P<0.05$. Student *t*-test or one-way ANOVA, followed by multiple-comparison Student Neuman-Keuls testing was performed to compare the data between two or three experimental groups, respectively. Two-way ANOVA using the MI and APLN status as the two independent variables (factors) was performed to compare the data between four experimental groups (WT, APLNKO, Sham and MI) (Figures 2E, 2F, 3, 4B through 4E, 4G through 4L, 7A, and 7C through 7F). We first confirmed that our data were normally distributed

(Shapiro-Wilk Statistic; $P<0.05$), and then performed the statistical analyses as noted above. Survival data were analyzed using the Kaplan-Meier method and the log-rank test was used to test for statistical significance (Figure 2B).

Results

Downregulation of APLN in Diseased Murine and Human Hearts

Acute MI, by ligation of the LAD artery, resulted in a drastic reduction in APLN levels in the infarct and peri-infarct regions at 1 day post-MI which persisted at 7 days post-MI. In contrast, APJ levels showed a bimodal change in the post-MI setting with an early increase followed by downregulation at 7 days post-MI (Figure 1A). In failing human hearts explanted following subacute MI, APLN levels showed a marked decrease with a corresponding increase in APJ levels (Figure 1B). Immunofluorescence staining confirmed a downregulation of APLN in the endothelial compartment of the infarcted murine and human hearts and in the myocardial interstitium with a concordant loss of APLN in epicardial coronary arteries in patients with coronary artery disease (Figures 1A, 1B, and S1).

Loss of APLN Enhances the Susceptibility to Myocardial Infarction

To ascertain whether APLN is a critical determinant of the cardiac response to ischemic injury, we subjected APLN knockout ($APLN^{-/y}$) and littermate wild-type ($APLN^{+/y}$) mice to MI. Western blot analysis confirmed loss of APLN in the absence of an upregulation of APJ levels in $APLN^{-/y}$ hearts (Figure 2A). Acute MI resulted in increased mortality in $APLN^{-/y}$ compared to $APLN^{+/y}$ mice based on Kaplan-Meier survival analysis with a 16% (8/50) and 32% (16/50) mortality, respectively (Figure 2B). The greater mortality in $APLN^{-/y}$ mice correlated with larger infarct size as demonstrated by TTC staining and greater elevation in plasma creatine kinase activity at 1 day post-MI (Figure 2C) leading to greater ventricular dilation and fibrosis (Figure 2D). Modulation of prosurvival pathways and angiogenesis are critical determinants of post-MI adverse myocardial remodeling.[34] APLN is an agonist of the G-protein coupled receptor, APJ, and can activate the well-known prosurvival kinase, PI3K/Akt. The TUNEL assay revealed a greater degree of apoptosis in the infarct-related region (Figure 2E) in 1-day post-MI $APLN^{-/y}$ hearts. Western blot analysis showed a consistent increase in phospho-Akt and Erk1/2 in the infarct, peri-infarct and

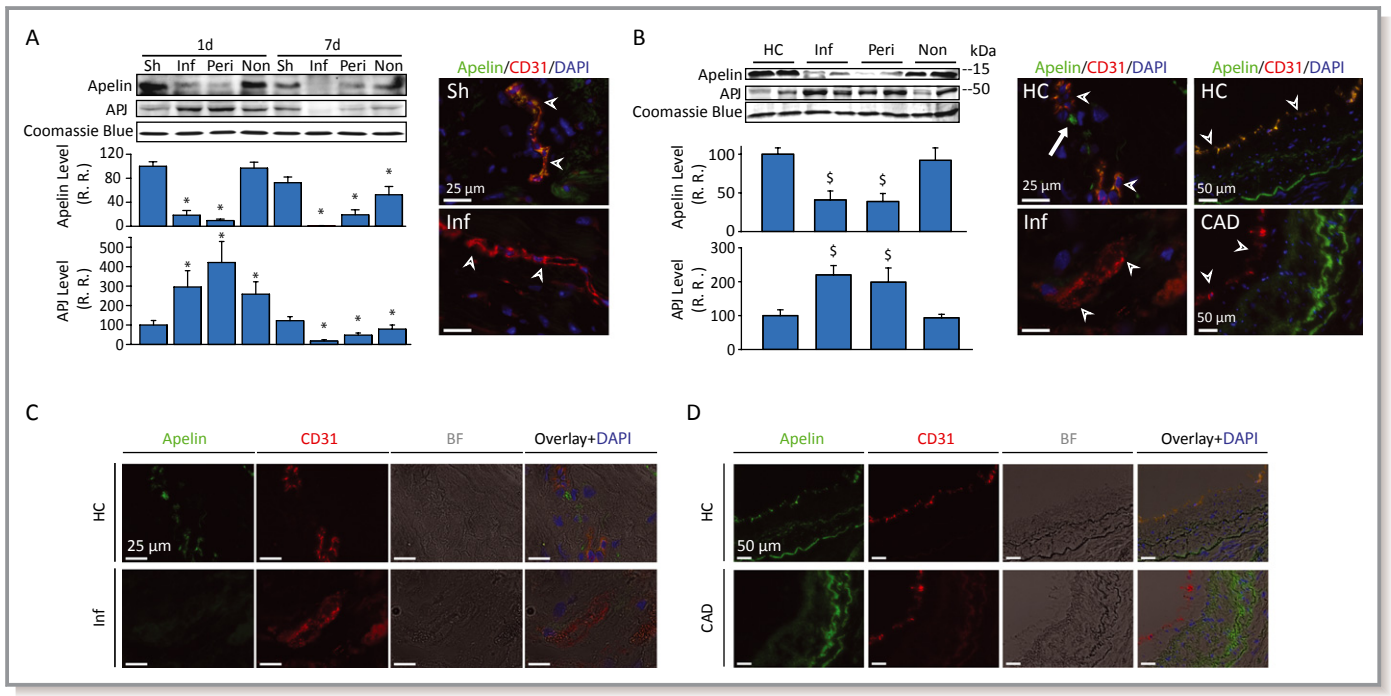

Figure 1. Myocardial apelin is downregulated in diseased murine and human hearts. Western blot analysis and immunofluorescence staining for apelin (green) and CD31 (red) illustrating marked loss of myocardial apelin in infarcted murine (A) and human hearts (B) with coronary artery disease (CAD) associated with a drastic loss of apelin in human epicardial coronary arteries (B). Immunofluorescence staining for apelin (green) and CD31 (red) with the individual brightfield images shown in the lower lane illustrating a marked loss of apelin in infarcted human myocardium (C) and in the left anterior descending coronary arteries from patients with CAD compared to healthy controls (HC) (D). The arrow indicates the human myocardial interstitium while the arrowheads illustrate the diseased human coronary endothelium. Sh indicates sham-operated; MI, myocardial infarction; Inf, infarct region; Peri, peri-infarct region; Non, non-infarct region; LAD, left anterior descending artery; R.R., relative ratio; LV, left ventricle; n=3; $^{*}P<0.05$ compared to the corresponding sham group; $^{\$}P<0.05$ compared with HCs and noninfarcted LV.

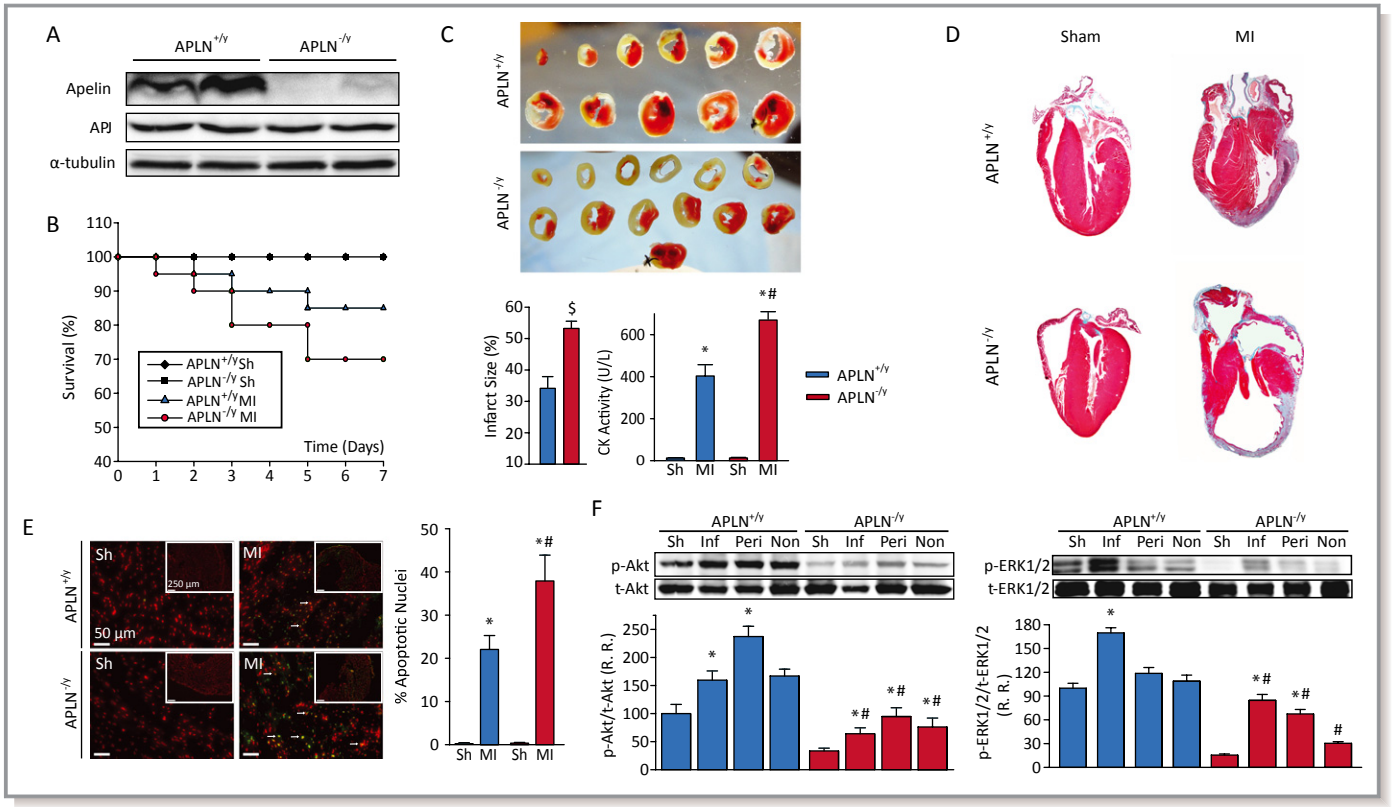

Figure 2. Loss of apelin enhances susceptibility to myocardial infarction. Western blot analysis of APLN and APJ levels showing a complete loss of APLN in APLN knockout ($APLN^{-/y}$) hearts without compensatory changes in APJ level (A). LAD-ligation resulting in increased mortality in $APLN^{-/y}$ mice based on Kaplan–Meier survival analysis (B), larger infarct size shown as representative images of triphenyl tetrazolium chloride (TTC)-stained heart sections and plasma creatine kinase (CK) activity at 1 day post-MI (C) and greater ventricular dilation and fibrosis at 7 day post-MI (D). TUNEL staining and quantification of apoptotic nuclei (E) revealed a greater increase in apoptosis in APLN-deficient hearts with Western blot analysis of serine-473 Akt and Erk1/2 phosphorylation showing increased levels at 1 day post-MI in $APLN^{+/y}$ hearts but with a dramatic loss of Akt and Erk1/2 phosphorylation in $APLN^{-/y}$ hearts (F). Sh indicates sham-operated; MI, myocardial infarction; Inf, infarct region; Peri, peri-infarct region; Non, noninfarct region; p, phospho; t, total; R.R., relative ratio; LAD, left anterior descending artery; APLN, Apelin. Values are mean±SEM; n=5 for each group except for B where n=50 ($P<0.01$ based on Kaplan–Meier survival analysis and log-rank test) and C where n=8. $^{\$}P<0.05$ compared to the corresponding sham group.*$P<0.05$ for the main effects and $^{\#}P<0.05$ for the interaction using two-way ANOVA.

noninfarct regions in $APLN^{+/y}$ hearts (Figure 2F). In contrast, loss of APLN resulted in a drastic lowering of phospho-Akt and Erk1/2 levels in the infarct and peri-infarct regions in $APLN^{-/y}$ hearts (Figure 2F). Increased cell death in $APLN^{-/y}$ hearts was also associated with greater neutrophil and macrophage infiltration (Figure 3A and 3B) associated with increased expression of proinflammatory cytokines (Figure 3C), and matrix metalloproteinases (MMPs), MMP8, MMP9 and MMP12 (Figure 3D) which will likely lead to degradation of the myocardial extracellular matrix.

The greater infarct size and increased myocardial inflammation coupled with compromised prosurvival signaling pathways likely contributes to worsened systolic dysfunction in APLN knockout mice. While baseline systolic function was not significantly different between $APLN^{+/y}$ and $APLN^{-/y}$ mice (Figure 4), which was confirmed at the single cardiomyocyte level (Figure S2), echocardiographic M-mode, parasternal long axis, and left atrial (Figure 4A) views showed worsening of systolic dysfunction, greater LV and left atrial dilation at 1 week post-MI in $APLN^{-/y}$ hearts. Quantitative assessment of systolic function showed increased left ventricular end-systolic volume (LVESV) (Figure 4B) and left atrial size (Figure 4C) with greater reduction in EF (Figure 4D) and worsening WMSI (Figure 4E) in APLN-deficient hearts. Invasive LV pressure-volume loop analysis confirmed equivalent basal systolic function and that $APLN^{-/y}$ mice showed a marked exacerbation of systolic dysfunction in response to MI independent of alterations in preload and afterload (Figure 4F through 4L).

Beneficial Effects of APLN Analogue in Myocardial Ischemic Injury

Exacerbation of post-MI dysfunction in APLN-deficient hearts suggests that enhancing APLN action can have salutary beneficial effects in ischemic heart disease. Given the short

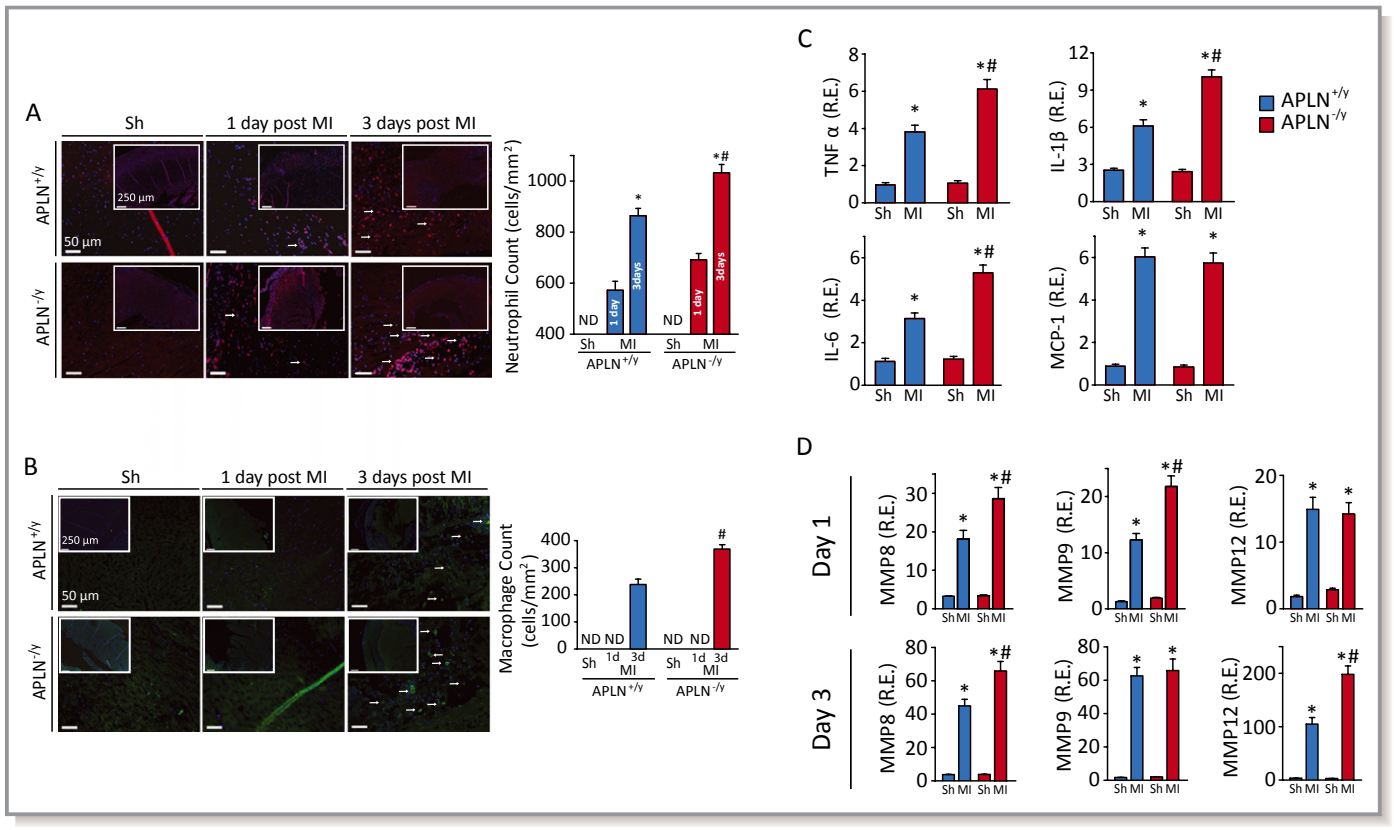

Figure 3. Increased myocardial inflammation following myocardial infarction in apelin-deficient hearts. Neutrophil-specific and macrophage-specific staining and quantification showing a greater increase in neutrophil (A) and macrophage infiltration (B) in infarcted APLN$^{-/y}$ compared to APLN$^{+/y}$ hearts. (C) Expression analysis of inflammatory cytokines and MMPs (matrix metalloproteinases) showing greater expression of tumor necrosis factor alpha (TNFα), interleukin 1beta (IL-1β), interleukin-6 (IL-6) and monocyte chemoattractant protein-1 (MCP-1) at 1 day post-MI in the infarct area of APLN knockout hearts. (D) Expression analysis of the inflammatory MMPs showing the neutrophil-specific MMPs, MMP8 and MMP9, were increased at 1 day post-MI while at day 3 post-MI, the macrophage-specific MMP, MMP12 level was increased in APLN-deficient hearts, R.E. (relative expression). Values are mean±SEM; n=6 for each sham group and n=8 for each MI group. *P<0.05 for the main effects and $^{\#}P$<0.05 for the interaction using two-way ANOVA. ND indicates not detected; Sh, sham-operated; MI, myocardial infarction; APLN, Apelin.

half-life of native APLN peptides,[11,24,35] we modified, synthesized and purified two novel APLN analogues with the aim to enhance their therapeutic effects: NleInpBrF pyr-1-apelin-13 (APLN analogue I) and NleAibBrF pyr-1-apelin-13 (APLN analogue II) (Figure S3; Tables S2 and S3). Using structure-activity relationships conducted on pyr-1-apelin,[36] we made multiple novel single amino acid substitutions combined into the same peptide with the aim of "masking" the susceptible C-terminal amide bond from proteolytic cleavage (APLN analogue I) or combined two potent APJ binding substitutions into the same peptide analogue while maintaining comparable stability to the native peptide (APLN analogue II). These analogues were purified using high-performance liquid chromatography (HPLC) (Figures S4 and S5), and high-resolution mass spectrometry and nuclear magnetic resonance (NMR) were used to confirm the sequence of the synthesized analogues (Figures S6 and S7). Proteolysis analysis using HPLC coupled with MALDI-TOF mass spectrometry confirmed efficient ACE2-mediated cleavage of pyr-1-apelin-13 (but not pyr-1-apelin-12) with 79.5±2.2%, 54.6±4.2% and 18.3±3.8% (n=3) of pyr-1-apelin-13 remaining at 30 s, 1 and 2 minutes following incubation with ACE2 (Figure S8) while APLN analogue I and analogue II were markedly resistant to ACE2-mediated proteolysis (Figure S9). We confirmed that APLN analogue I and II were not inhibitors of ACE2 activity (Figure S10) and as such the lack of formation of degradation products is due to the intrinsic resistance of the APLN analogues to ACE2 action.

We used the ex vivo Langendorff heart preparation to further determine the role of APLN in myocardial ischemic injury and to evaluate the therapeutic effects of the synthetic APLN analogues. Notably, in response to myocardial IR injury, APLN$^{-/y}$ hearts exhibited suppressed functional recovery compared to APLN$^{+/y}$ hearts as illustrated by representative hemodynamic responses (Figure 5A), LV developed pressure (Figure 5B), rate-pressure product (Figure 5C) and measures of myocardial contractility, dP/dt_{max}, and dP/dt_{min} (Figure 5D). The enhanced susceptibility to IR injury is consistent with the reduced viability of adult cardiomyocytes isolated from APLN-deficient hearts (Figure 6A and 6B).

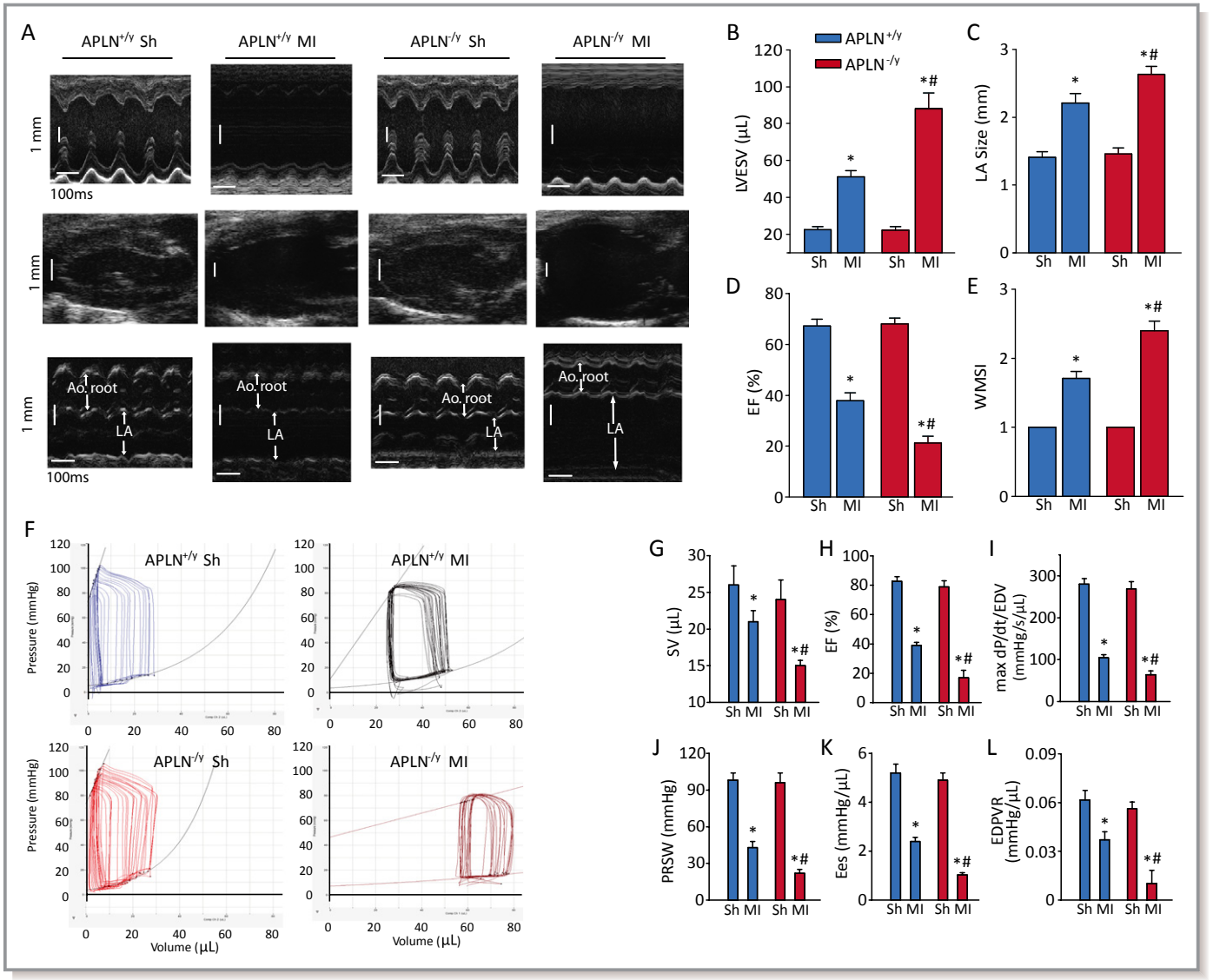

Figure 4. Echocardiographic and invasive pressure-volume assessment of heart function revealed increased left ventricular dilation and dysfunction post-MI in apelin-deficient hearts. Representative M-mode images, parasternal long axis views and left atrial size (A) from APLN$^{+/y}$ and APLN$^{-/y}$ hearts after sham or 1 week post-MI with greater increase in left ventricular end-systolic volume (LVESV) (B) and left atrial (LA) size (C) with lowering of the ejection fraction (EF) (D) and worsening wall motion score index (WMSI) (E) in APLN$^{-/y}$ hearts compared with APLN$^{+/y}$ hearts at 1 week post-MI. Invasive pressure-volume hemodynamic analysis showing marked deterioration in the post-MI ventricular function in apelin-deficient hearts (F) with quantitative assessment of LV function showing reduced stroke volume (SV) (G), EF (H), max dP/dt/EDV (I), preload recruitable stroke work (PRSW) (J) and end-systolic elastance (Ees) (K) with decreased slope of the end-diastolic pressure volume relationship (EDPVR) (L). Sh indicates sham-operated; MI, myocardial infarction; EDV, end diastolic volume; APLN, Apelin. Values are mean±SEM; n=8 for each sham group and n=10 for each MI group. *P<0.05 for the main effects and $^{\#}P$<0.05 for the interaction using two-way ANOVA.

A postconditioning protocol was used in which APLN analogues were applied following the ischemic period in APLN$^{+/y}$ (wildtype) hearts in order to simulate a potential clinical application. While APLN analogue I (1 μmol/L) failed to prevent the IR injury (Figure 6C through 6E), APLN analogue II (1 μmol/L) resulted in a greater recovery of function as illustrated by representative hemodynamic responses (Figure 5A) and the quantitative measure of myocardial performance (Figure 5B through 5D). Analysis of creatine kinase activity in the coronary perfusate corroborated the greater myocardial damage in the reperfused APLN$^{-/y}$ hearts with a marked protection seen in response to APLN analogue II (Figure 5E). The increased phosphorylation of Akt and Erk1/2, two critical pathways in mediating cardioprotection against myocardial IR injury,[37] were reduced in the absence of APLN at 10 minutes (Figure 5F) and at 40 minutes postreperfusion (Figure S11) with APLN analogue II leading to greater activation of these protective signaling pathways (Figure 5F). Next, we extrapolated our findings to an in vivo model of IR injury in which the proximal LAD coronary

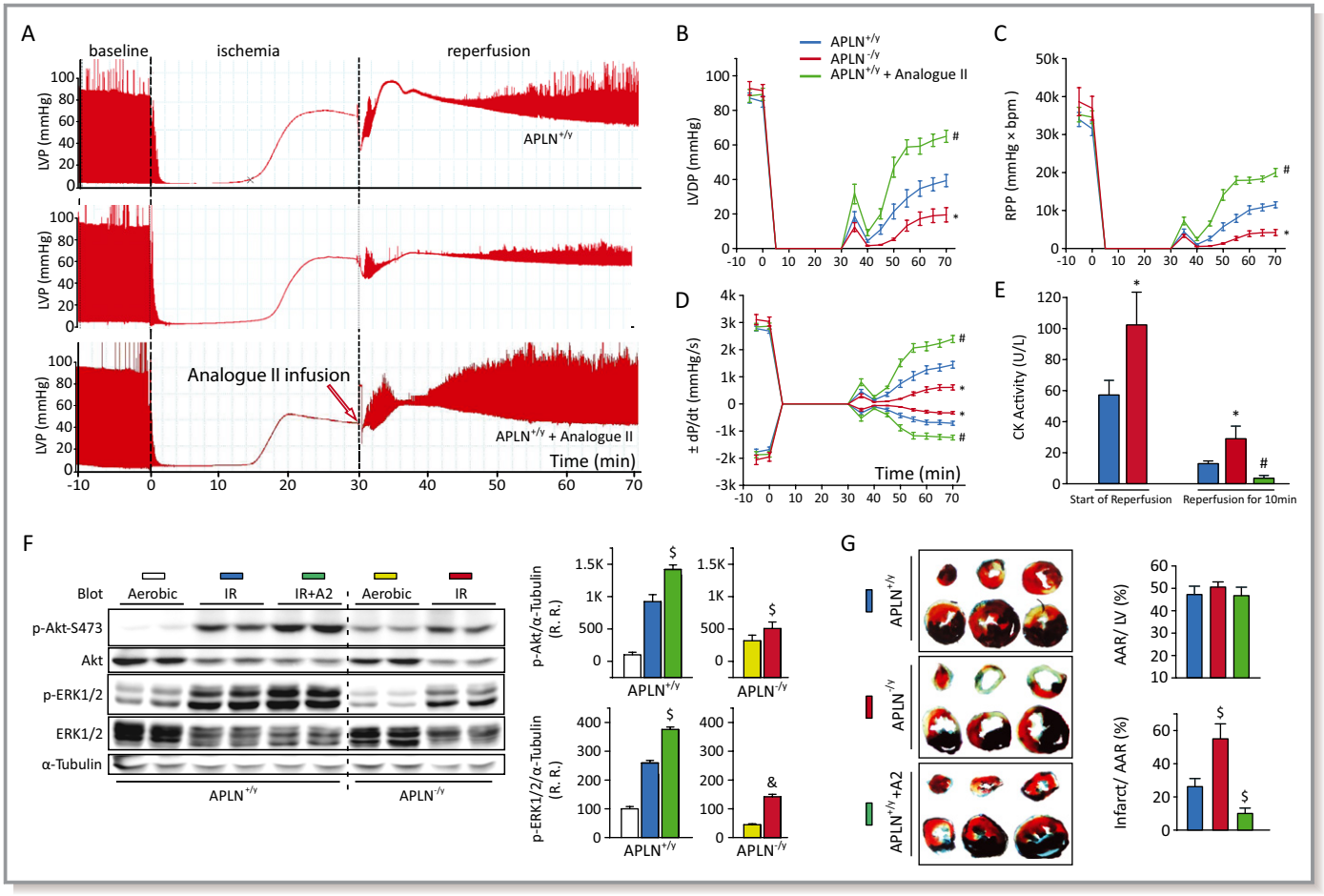

Figure 5. Myocardial ischemia-reperfusion injury using the ex vivo Langendorff system is exacerbated by the absence of apelin and is rescued by apelin analogue. (A) Representative hemodynamic tracings of APLN$^{+/y}$ and APLN$^{-/y}$ hearts showing a marked reduction in post-ischemic functional recovery of APLN$^{-/y}$ hearts with a dramatic protection in response to apelin analogue II (1.5 μg/mL for 20 minutes) at the start of reperfusion. Functional assessment of the LV developed pressure (LVDP) (B), rate-pressure product (RPP) (C), maximum and minimum rate of change in LV pressure ($\pm$dP/dt) (D) showing marked suppression of post-ischemic functional recovery in apelin-deficient hearts and a dramatic protection in response to apelin analogue II. (E) Creatine kinase activity in the coronary perfusate showing a marked increase in APLN$^{-/y}$ compared to APLN$^{+/y}$ hearts at the start and after 10 minutes of reperfusion with reduced damage in response to apelin analogue II. (F) Western blot analysis of serine-473 Akt and Erk1/2 phosphorylation showing increased phosphorylation in response to ischemia-reperfusion (IR) injury in APLN$^{+/y}$ hearts which was markedly suppressed by loss of APLN and further stimulated by apelin analogue II. (G) In vivo IR due to 30 minutes ischemia in the LAD territory followed by 3 hours reperfusion with Evan's blue and TTC staining showing greater infarct size in APLN$^{-/y}$ hearts and a marked reduction in infarct size in response to apelin analogue II (2 μg/min for 10 minutes i.v.) at the start of reperfusion. p indicates phospho; LVP, left ventricular pressure; A2, analogue II; t, total; R.R., relative ratio; AAR, area at risk; APLN, Apelin; LV, left ventricle; IR, ischemia-reperfusion; LAD, left anterior descending artery; TTC, triphenyl tetrazolium chloride; CK, creatine kinase. Values are mean $\pm$SEM; n=8 per groups except for F where n=5. *P<0.05 compared to the APLN$^{+/y}$ group; $^{\#}P$<0.05 compared to all other groups; $^{\$}P$<0.05 compared with the APLN$^{+/y}$ IR group and $^{\&}P$<0.05 compared with corresponding aerobic group.

artery was occluded for 30 minutes followed by 3 hours of reperfusion. While loss of APLN resulted in a greater infarct size, APLN analogue II administered at the time of perfusion significantly reduced the in vivo IR injury in APLN$^{+/y}$ hearts (Figure 5G).

Critical Role of APLN in Myocardial Angiogenesis: Stimulation by APLN Analogue

APLN stimulates the angiogenic response, a key adaptive mechanism in ischemic heart disease and a determinant of infarct expansion.[34,38,39] We next examined the role of APLN in the adaptive angiogenesis response. Nuclear translocation of the key transcription factor, HIF-1α, was reduced in the infarct region as delineated by immunofluorescence staining (Figure 7A) and Western blot analysis (Figure 7B) resulting in a lack of upregulation of VEGF in the infarcted APLN-deficient myocardium (Figure 7C). While the regional expression of angiopoeitin-1 (Ang-1) was not differentially affected, angiopoetin-2 (Ang-2) levels were decreased in infarcted APLN$^{-/y}$ hearts at 3 days post-MI (Figure 7D). Collectively, these data show a clear and important role of angiogenesis and as such

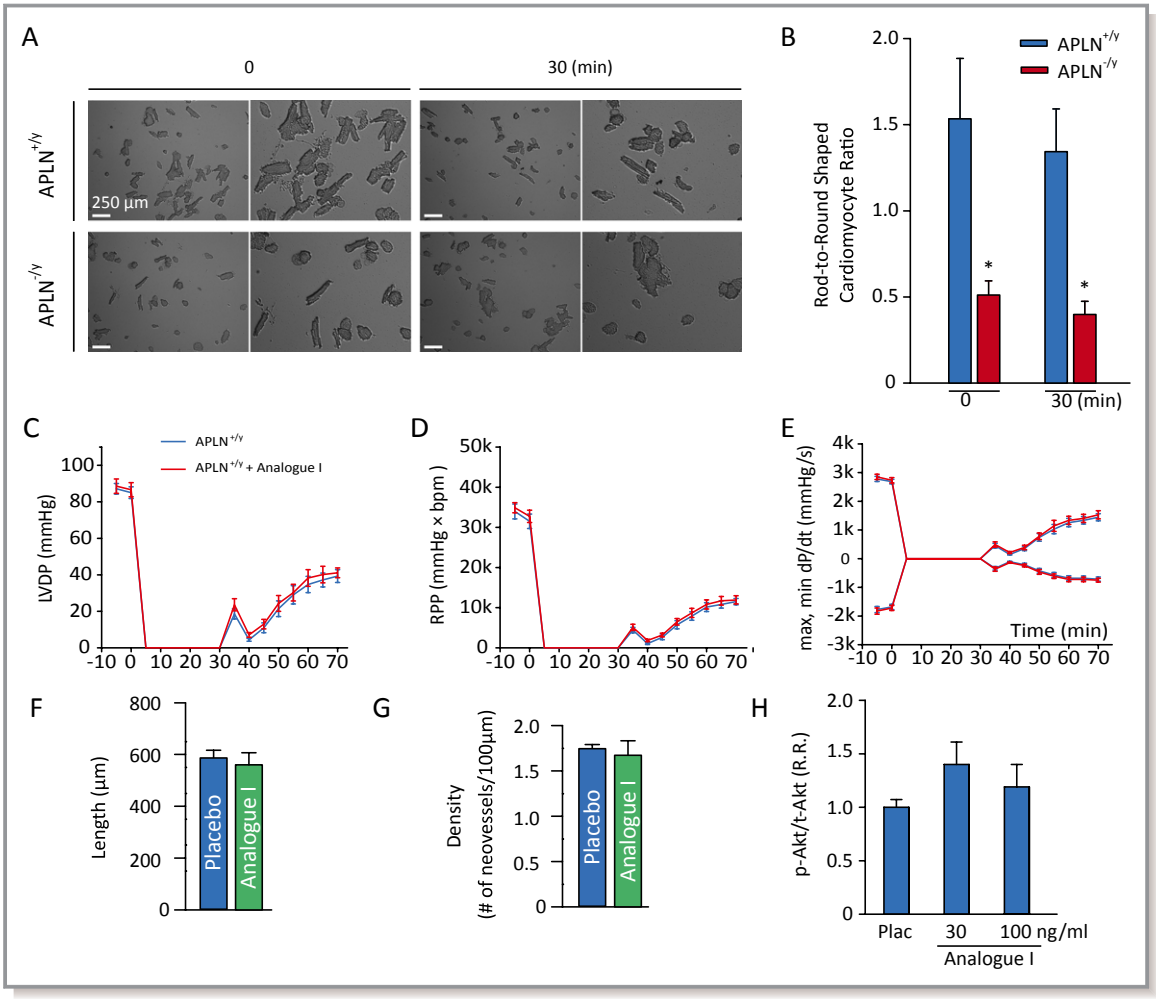

Figure 6. Reduced viability of cardiomyocytes isolated from APLN-deficient hearts and lack of biological effects of Apelin analogue I. Reduced viability of isolated adult cardiomyocytes from APLN$^{-/y}$ hearts compared with wildtype APLN$^{+/y}$ as illustrated by morphological assessment (A, B). Apelin analogue I (NleInpBrF pyr-1-apelin-13) given at 1.5 μg/mL for 20 minutes into the coronary circulation of WT mice at the time of reperfusion failed to protect the ex vivo wildtype hearts from ischemia-reperfusion injury (C, E) and was unable to stimulate angiogenesis (F, G) or Akt phosphorylation in human EPCs at 100 ng/mL (H). LVDP indicates left ventricle developed pressure; APLN, Apelin; RPP, rate-pressure product; dP/dt, rate of change in LV pressure; p, phospho; t, total; R.R., relative ratio. Values are mean ±SEM; n=8 per groups except for H where n=5. *P<0.05 compared with the APLN$^{+/y}$ group.

we examined the in situ angiogenic response in the post-MI heart using CD31 immunofluorescence (Figure 7E) and lectin staining (Figure 7F) of the coronary endothelial cells and microvasculature, respectively. Our results show a marked reduction in capillary density and vessel integrity in the post-MI APLN$^{-/y}$ hearts compared to APLN$^{+/y}$ hearts (Figure 7E and 7F).

We used the aortic ring culture method and showed that vessel sprouting was impaired in APLN-deficient vessels, which was rescued by supplementation with APLN analogue II and recombinant human VEGF (Figure 8A). To further substantiate the role of APLN in angiogenesis, we isolated and purified hEPCs and confirmed the endothelial lineage by flow-cytometry for the endothelial-specific marker, VE-cadherin and expression of Von Willebrand factor and eNOS (Figure 8B). siRNA knockdown of APLN in hEPCs reduced APLN expression by ~80% (Figure 8C) and using an in vitro angiogenesis culture, expression of characteristic tip cell genes revealed markedly decreased expression of DLL4 (Figure 8D), a gene implicated in directing the tip versus stalk cell phenotype[40–42] without affecting Flt1 and KDR expression (Figure S12). Silencing of APLN function disrupted endothelial sprouting with increased short/long vessel ratio and reduced endothelial sprout density correlating with a marked suppression of DLL4 (Figure 8E). Importantly, APLN analogue II stimulated the endothelial sprouting resulting in longer capillary tube formation (Figure 8E) in association with increased phospho-Akt in hEPCs (Figure 8F). In contrast, APLN analogue I failed to alter the angiogenic response and Akt phosphorylation of hEPCs (Figure 6F

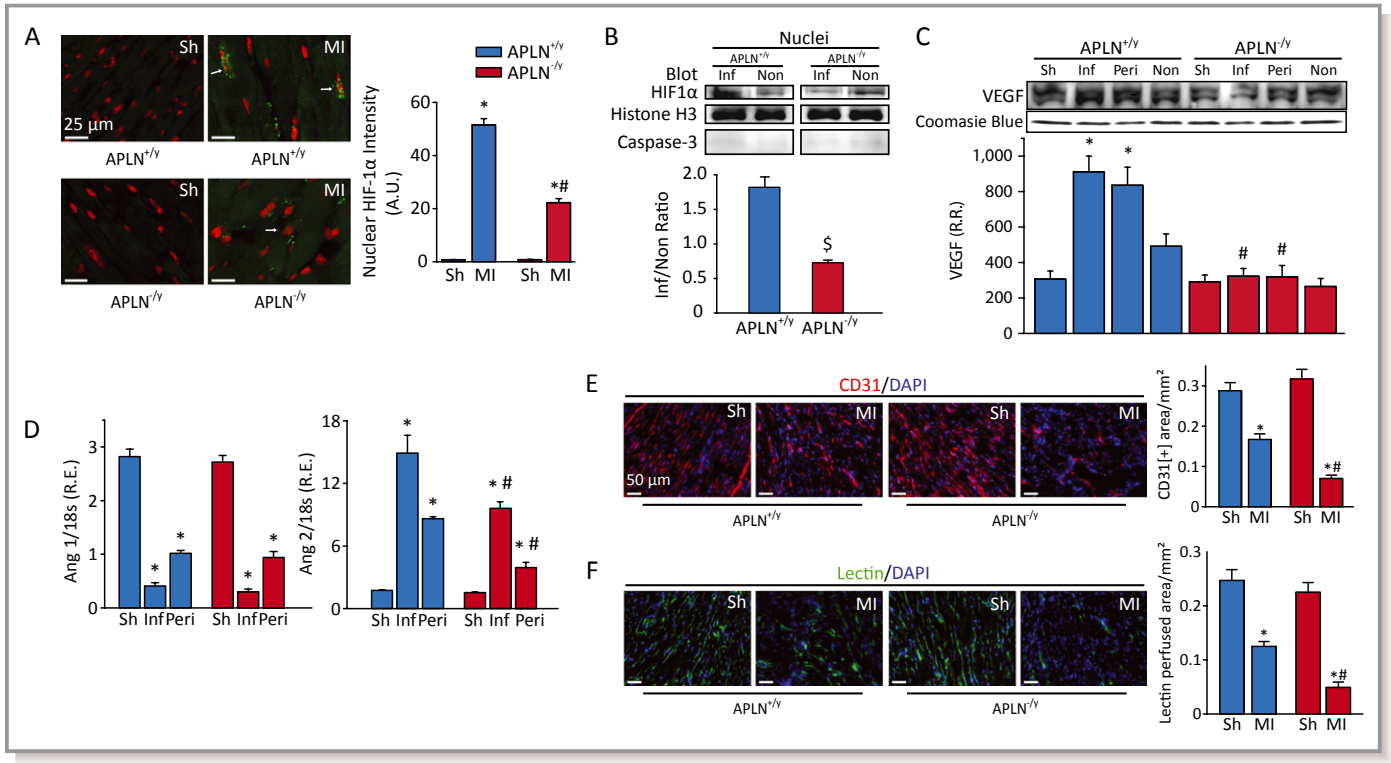

Figure 7. Disruption of apelin impairs the in vivo angiogenic response. Immunofluorescence staining for HIF-1α showing lowered levels of HIF-1α with decrease in nuclear translocation (A) which was confirmed by Western blot analysis of nuclear HIF-1α (relative to cytosolic) (B) in response to myocardial infarction in APLN$^{-/y}$ hearts. (C) Western blot analysis of VEGF levels in 1-day post-infarcted hearts showing a significant increase in APLN$^{+/y}$ hearts which was absent in APLN$^{-/y}$ hearts. (D) Regional expression analysis of angiopoeitin-1 (Ang-1) and angiopoetin-2 (Ang-2) levels in APLN$^{+/y}$ and APLN$^{-/y}$ post-infarcted hearts showing reduced Ang-2 levels in apelin-deficient hearts. In situ assessment and quantification of angiogenesis in 7-day post-MI hearts by using CD31 staining of the coronary endothelial cells (E) and lectin immunofluorescence of the coronary vasculature (F) showing a greater loss of endothelial cells and vascular integrity in apelin-deficient hearts. Sh indicates sham-operated; APLN, Apelin; MI, myocardial infarction; Inf, infarct region; Peri, peri-infarct region; Non, non-infarct region; p, phospho; t, total; R.R., relative ratio; VEGF, vascular endothelial growth factor; HIF-1α, hypoxia inducible factor-1 alpha. n=5 except for D where n=8. $^{\$}P<0.05$ compared to the APLN$^{+/y}$ group.$^{*}P<0.05$ for the main effects and $^{\#}P<0.05$ for the interaction using two-way ANOVA.

through 6H). These findings confirmed that APLN deficiency inhibits the angiogenic response in the post-MI heart and in hEPCs.

Discussion

Coronary artery disease characterized by adverse post-MI remodeling and IR injury is now the most common cause of heart failure.[12,37] We showed the APLN/APJ pathway is drastically altered in post-MI myocardial tissue characterized by a marked reduction in APLN levels in murine hearts. Importantly, in explanted human hearts with primary ischemic injury, there was a marked loss of APLN in various compartments confirming a critical role of APLN in human heart failure secondary to ischemic heart disease. Using a genetic model we showed that loss of APLN impaired post-MI remodeling, angiogenesis and functional recovery, and exacerbated myocardial IR injury ex vivo and in vivo demonstrating a critical causal role of APLN in myocardial ischemic injury. The loss of APLN clearly compromises the activation of the protective Akt/PI3K[43] and Erk1/2 signaling pathways,[44] both in vivo and ex vivo, resulting in increased myocardial damage and worsening heart function. Our synthetic apelin analogue provided salutary beneficial effects against ex vivo and in vivo myocardial injury. The C-terminal phenylalanine residue of apelin-13 is essential for activity and its removal leads to a 10-fold decrease in binding and functional efficacy.[36,45] We have shown that in contrast to pyr-1-apelin-13, APLN analogue I and II were extremely resistant to proteolytic cleavage of the C-terminal phenylalanine by ACE2. The ability of APLN analogue II to improve both systolic and diastolic function is particularly useful in the setting of myocardial ischemia. In addition to the prosurvival effects of APLN and APLN analogues, the ability of these agonists to activate Akt and eNOS[15,46] can directly improve the contractility and relaxation of the cardiomyocytes.[47,48]

Genetic variation in the APJ receptor modifies the progression of heart failure in patients with dilated cardiomyopathy.[9]

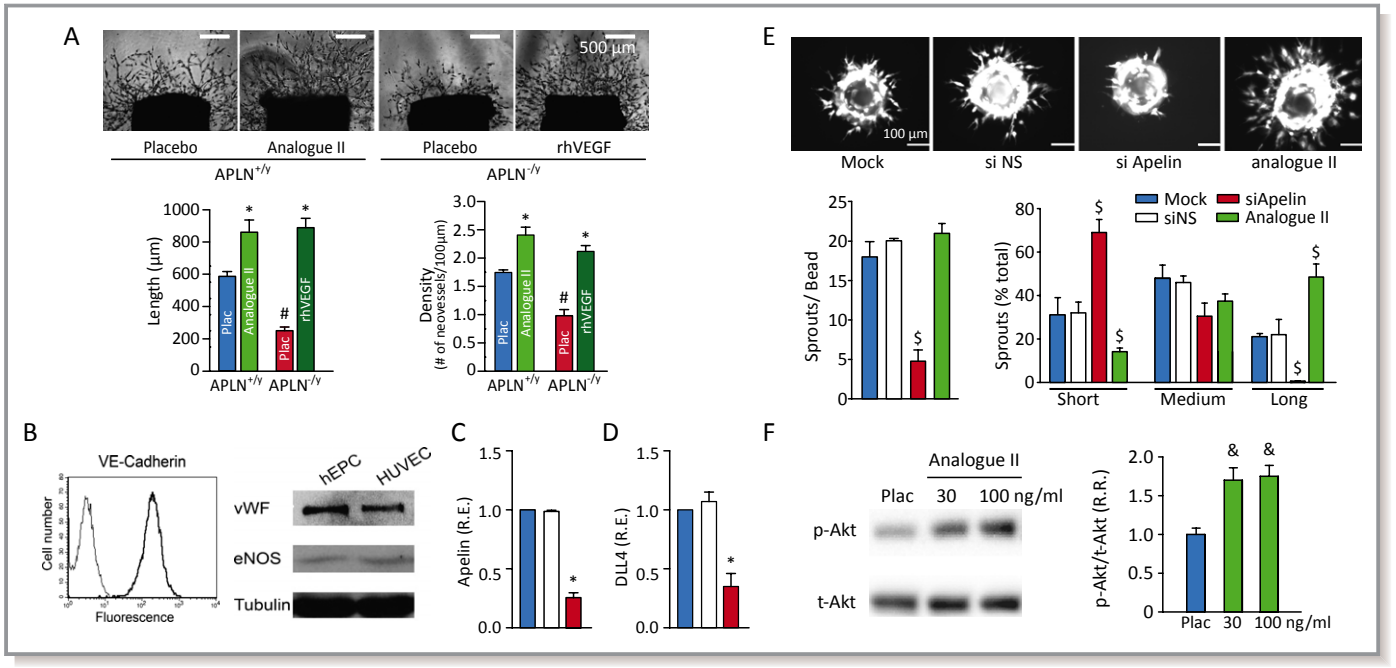

Figure 8. Loss of apelin impairs the in vitro angiogenic response in murine aorta and human endothelial progenitor cells while apelin analogue stimulates angiogenesis. (A) Representative aortic ring cultures from APLN$^{+/y}$ and APLN$^{-/y}$ mice showing a marked decrease in sprout length and density which was rescued by supplementation with apelin analogue II (100 ng/mL) and rhVEGF (20 ng/mL). (B) Characterization of the isolated human endothelial progenitor cells (hEPCs) using flow cytometry of the endothelial-specific marker, VE-cadherin while Western blot analysis of von Willebrand factor (vWF) and eNOS showed comparable expression with a positive control, human umbilical vein endothelial cells (HUVEC). Transfection of human endothelial progenitor cells with a non-silencing control siRNA (siNS) or siRNA against apelin (siApelin) resulting in 80% decrease in apelin (C) and DLL4 (D) expression. (E) Representative beads and quantification of sprout length based on tertiles established from mock-transfected hEPC (Mock) and sprout density showing a drastic reduction in endothelial sprout density and sprout lengthening with knockdown of apelin. Apelin analogue II (100 ng/mL) stimulates endothelial lengthening (E) and increased phospho-Akt (serine-473) in hEPCs (F). rhVEGF indicates recombinant human vascular endothelial growth factor; APLN, Apelin; NS, nonsense; p, phospho; t, total; R.R., relative ratio; eNOS, endothelial nitric oxide synthase. Values are mean±SEM; n=5 for each group. *P<0.05 compared to the corresponding sham/placebo group; $^{\#}P$<0.05 compared to the APLN$^{+/y}$ group; $^{\$}P$<0.05 compared to all other groups and $^{\&}P$<0.05 compared with placebo.

In Dahl salt-sensitive hypertensive (DS) rats, cardiac APLN /APJ pathway is markedly downregulated with the onset of heart failure.[49] APLN mediates positive inotropic effect in vitro[5,6] and in vivo[7] and minimizes increases in systemic arterial and venous tone[2–4] with corresponding reductions in LV afterload and preload. The integrative physiological role of the APLN system strongly suggest that enhancing APLN action may serve to minimize myocardial ischemic damage and the progression to advanced heart failure.[7,11] The APLN/APJ signaling pathway is downstream of Cripto, a member of the EGF-CFC family of signaling molecules, promotes cardiomyocyte differentiation[50] and enhanced cardiac differentiation of embryonic stem cells[51], processes which may be recruited in the post-MI setting. Using in vitro and in vivo assessment of angiogenesis, we showed that APLN is required for normal angiogenesis, a key adaptive mechanism in ischemic and pressure-overload–induced heart failure.[38,39,52] We observed a marked deficiency in angiogenic sprout formation in a robust assay of 3-dimensional angiogenesis using primary hEPCs when APLN was silenced. APLN induces phosphorylation of eNOS and NO release from endothelial cells thereby stimulating angiogenesis[13] while loss of APLN may sensitize endothelial cells to apoptosis.[13,53] As such, the APLN/APJ system has emerged as a critical mediator of the spatial and temporal control of angiogenesis in heart disease. Our study has several limitations. We used a germ-line knockout of APLN and therefore we cannot distinguish cell-specific effects of APLN action versus the systemic changes associated with a whole-body knockout of apelin. In addition, a detailed molecular pharmacological characterization of the APLN analogues including in vivo pharmacokinetics and their binding properties to their cognate receptors is needed and we cannot exclude off-target effects of the APLN analogues given the concentrations used in this study.

Collectively, our results and previous studies have delineated a critical role of the APLN/APJ axis in the regulation of cardiovascular functions and fluid homeostasis. APLN increases cardiac contractility in vitro[5,6] and in vivo[7] and minimizes increases in systemic arterial and venous tone[2–4] with corresponding reductions in LV afterload and preload. In addition, APLN receptor agonism mediates central effect and suppresses arginine vasopressin[54] thereby promoting renal fluid loss which may be particularly attractive in patients

with HF. Since the APLN/APJ system is compromised in human heart failure,[3,10] the integrative physiological role of the APLN/APJ system strongly suggest that enhancing APLN action may serve to minimize myocardial ischemic damage and the progression to advanced heart failure. Enhancing APLN action represents a new potential drug target for the treatment of ischemic heart failure. The short half-life of native APLN peptides[11,24,35] implies a need to generate APLN analogues which are more potent and less susceptible to degradation. Our ability to design and synthesize novel APLN analogues illustrate that APLN can be targeted pharmacologically to enhance the therapeutic effects and to provide potential drugs.

Sources of Funding

This study was supported by an operating grant from Canadian Institute for Health Research (grant 86602 to Dr Oudit; grant 53319 to Dr Murray), Alberta Innovates-Health Solutions (to Drs Basu, Kandalam, Kassiri, Vederas, and Oudit), Natural Sciences and Engineering Research Council of Canada (to Dr Vederas), EuGeneHeart (EU 6th Framework Programs), the Austrian National Bank, and the Institute of Molecular Biotechnology, Austria (to Dr Penninger).

Disclosures

None.

References

1. Tatemoto K, Hosoya M, Habata Y, Fujii R, Kakegawa T, Zou MX, Kawamata Y, Fukusumi S, Hinuma S, Kitada C, Kurokawa T, Onda H, Fujino M. Isolation and characterization of a novel endogenous peptide ligand for the human APJ receptor. *Biochem Biophys Res Commun*. 1998;251:471–476.
2. Pitkin SL, Maguire JJ, Bonner TI, Davenport AP. International union of basic and clinical pharmacology. LXXIV. Apelin receptor nomenclature, distribution, pharmacology, and function. *Pharmacol Rev*. 2010;62:331–342.
3. Chen MM, Ashley EA, Deng DX, Tsalenko A, Deng A, Tabibiazar R, Ben-Dor A, Fenster B, Yang E, King JY, Fowler M, Robbins R, Johnson FL, Bruhn L, McDonagh T, Dargie H, Yakhini Z, Tsao PS, Quertermous T. Novel role for the potent endogenous inotrope apelin in human cardiac dysfunction. *Circulation*. 2003;108:1432–1439.
4. Kleinz MJ, Skepper JN, Davenport AP. Immunocytochemical localisation of the apelin receptor, APJ, to human cardiomyocytes, vascular smooth muscle and endothelial cells. *Regul Pept*. 2005;126:233–240.
5. Wang C, Du JF, Wu F, Wang HC. Apelin decreases the SR Ca2+ content but enhances the amplitude of [Ca2+]i transient and contractions during twitches in isolated rat cardiac myocytes. *Am J Physiol Heart Circ Physiol*. 2008;294:H2540–2546.
6. Szokodi I, Tavi P, Foldes G, Voutilainen-Myllyla S, Ilves M, Tokola H, Pikkarainen S, Piuhola J, Rysa J, Toth M, Ruskoaho H. Apelin, the novel endogenous ligand of the orphan receptor APJ, regulates cardiac contractility. *Circ Res*. 2002;91:434–440.
7. Berry MF, Pirolli TJ, Jayasankar V, Burdick J, Morine KJ, Gardner TJ, Woo YJ. Apelin has in vivo inotropic effects on normal and failing hearts. *Circulation* 2004;110:II187–II193.
8. Pitkin SL, Maguire JJ, Kuc RE, Davenport AP. Modulation of the apelin/APJ system in heart failure and atherosclerosis in man. *Br J Pharmacol*. 2010;160:1785–1795.
9. Sarzani R, Forleo C, Pietrucci F, Capestro A, Soura E, Guida P, Sorrentino S, Iacoviello M, Romito R, Dessi-Fulgheri P, Pitzalis M, Rappelli A. The 212A variant of the APJ receptor gene for the endogenous inotrope apelin is associated with slower heart failure progression in idiopathic dilated cardiomyopathy. *J Card Fail*. 2007;13:521–529.
10. Chong KS, Gardner RS, Morton JJ, Ashley EA, McDonagh TA. Plasma concentrations of the novel peptide apelin are decreased in patients with chronic heart failure. *Eur J Heart Fail*. 2006;8:355–360.
11. Japp AG, Cruden NL, Barnes G, van Gemeren N, Mathews J, Adamson J, Johnston NR, Denvir MA, Megson IL, Flapan AD, Newby DE. Acute cardiovascular effects of apelin in humans: potential role in patients with chronic heart failure. *Circulation*. 2010;121:1818–1827.
12. Go AS, Mozaffarian D, Roger VL, Benjamin EJ, Berry JD, Borden WB, Bravata DM, Dai S, Ford ES, Fox CS, Franco S, Fullerton HJ, Gillespie C, Hailpern SM, Heit JA, Howard VJ, Huffman MD, Kissela BM, Kittner SJ, Lackland DT, Lichtman JH, Lisabeth LD, Magid D, Marcus GM, Marelli A, Matchar DB, McGuire DK, Mohler ER, Moy CS, Mussolino ME, Nichol G, Paynter NP, Schreiner PJ, Sorlie PD, Stein J, Turan TN, Virani SS, Wong ND, Woo D, Turner MB. Heart disease and stroke statistics–2013 update: a report from the American Heart Association. *Circulation*. 2013;127:e6–e245.
13. Kidoya H, Ueno M, Yamada Y, Mochizuki N, Nakata M, Yano T, Fujii R, Takakura N. Spatial and temporal role of the apelin/APJ system in the caliber size regulation of blood vessels during angiogenesis. *EMBO J*. 2008;27:522–534.
14. Kidoya H, Naito H, Takakura N. Apelin induces enlarged and nonleaky blood vessels for functional recovery from ischemia. *Blood*. 2010;115:3166–3174.
15. Tao J, Zhu W, Li Y, Xin P, Li J, Liu M, Redington AN, Wei M. Apelin-13 protects the heart against ischemia-reperfusion injury through inhibition of ER-dependent apoptotic pathways in a time-dependent fashion. *Am J Physiol Heart Circ Physiol*. 2011;301:H1471–1486.
16. Kuba K, Zhang L, Imai Y, Arab S, Chen M, Maekawa Y, Leschnik M, Leibbrandt A, Markovic M, Schwaighofer J, Beetz N, Musialek R, Neely GG, Komnenovic V, Kolm U, Metzler B, Ricci R, Hara H, Meixner A, Nghiem M, Chen X, Dawood F, Wong KM, Sarao R, Cukerman E, Kimura A, Hein L, Thalhammer J, Liu PP, Penninger JM. Impaired heart contractility in apelin gene-deficient mice associated with aging and pressure overload. *Circ Res*. 2007;101:e32–42.
17. Kassiri Z, Zhong J, Guo D, Basu R, Wang X, Liu PP, Scholey JW, Penninger JM, Oudit GY. Loss of angiotensin-converting enzyme 2 accelerates maladaptive left ventricular remodeling in response to myocardial infarction. *Circ Heart Fail*. 2009;2:446–455.
18. Gao E, Lei YH, Shang X, Huang ZM, Zuo L, Boucher M, Fan Q, Chuprun JK, Ma XL, Koch WJ. A novel and efficient model of coronary artery ligation and myocardial infarction in the mouse. *Circ Res*. 2010;107:1445–1453.
19. Kandalam V, Basu R, Abraham T, Wang X, Soloway PD, Jaworski DM, Oudit GY, Kassiri Z. TIMP2 deficiency accelerates adverse post-myocardial infarction remodeling because of enhanced MT1-MMP activity despite lack of MMP2 activation. *Circ Res*. 2010;106:796–808.
20. Zhang Y, Takagawa J, Sievers RE, Khan MF, Viswanathan MN, Springer ML, Foster E, Yeghiazarians Y. Validation of the wall motion score and myocardial performance indexes as novel techniques to assess cardiac function in mice after myocardial infarction. *Am J Physiol Heart Circ Physiol*. 2007;292:H1187–1192.
21. Cerqueira MD, Weissman NJ, Dilsizian V, Jacobs AK, Kaul S, Laskey WK, Pennell DJ, Rumberger JA, Ryan T, Verani MS. Standardized myocardial segmentation and nomenclature for tomographic imaging of the heart: a statement for healthcare professionals from the Cardiac Imaging Committee of the Council on Clinical Cardiology of the American Heart Association. *Circulation*. 2002;105:539–542.
22. Pacher P, Nagayama T, Mukhopadhyay P, Batkai S, Kass DA. Measurement of cardiac function using pressure-volume conductance catheter technique in mice and rats. *Nat Protoc*. 2008;3:1422–1434.
23. Porterfield JE, Kottam AT, Raghavan K, Escobedo D, Jenkins JT, Larson ER, Trevino RJ, Valvano JW, Pearce JA, Feldman MD. Dynamic correction for parallel conductance, GP, and gain factor, alpha, in invasive murine left ventricular volume measurements. *J Appl Physiol*. 2009;107:1693–1703.
24. Vickers C, Hales P, Kaushik V, Dick L, Gavin J, Tang J, Godbout K, Parsons T, Baronas E, Hsieh F, Acton S, Patane M, Nichols A, Tummino P. Hydrolysis of biological peptides by human angiotensin-converting enzyme-related carboxypeptidase. *J Biol Chem*. 2002;277:14838–14843.
25. Baker M, Robinson SD, Lechertier T, Barber PR, Tavora B, D'Amico G, Jones DT, Vojnovic B, Hodivala-Dilke K. Use of the mouse aortic ring assay to study angiogenesis. *Nat Protoc*. 2012;7:89–104.
26. Ingram DA, Mead LE, Tanaka H, Meade V, Fenoglio A, Mortell K, Pollok K, Ferkowicz MJ, Gilley D, Yoder MC. Identification of a novel hierarchy of endothelial progenitor cells using human peripheral and umbilical cord blood. *Blood*. 2004;104:2752–2760.

27. Nakatsu MN, Hughes CC. An optimized three-dimensional in vitro model for the analysis of angiogenesis. *Methods Enzymol*. 2008;443:65–82.
28. Zhang QX, Nakhaei-Nejad M, Haddad G, Wang X, Loutzenhiser R, Murray AG. Glomerular endothelial PI3 kinase-alpha couples to VEGFR2, but is not required for eNOS activation. *Am J Physiol Renal Physiol*. 2011;301:F1242–1250.
29. Guo D, Kassiri Z, Basu R, Chow FL, Kandalam V, Damilano F, Liang W, Izumo S, Hirsch E, Penninger JM, Backx PH, Oudit GY. Loss of PI3K{gamma} enhances cAMP-dependent MMP remodeling of the myocardial N-cadherin adhesion complexes and extracellular matrix in response to early biomechanical stress. *Circ Res*. 2010;107:1275–1289.
30. Zhong J, Basu R, Guo D, Chow FL, Byrns S, Schuster M, Loibner H, Wang XH, Penninger JM, Kassiri Z, Oudit GY. Angiotensin-converting enzyme 2 suppresses pathological hypertrophy, myocardial fibrosis, and cardiac dysfunction. *Circulation*. 2010;122:717–728.
31. Patel VB, Bodiga S, Fan D, Das SK, Wang Z, Wang W, Basu R, Zhong J, Kassiri Z, Oudit GY. Cardioprotective effects mediated by angiotensin II type 1 receptor blockade and enhancing angiotensin 1-7 in experimental heart failure in angiotensin-converting enzyme 2-null mice. *Hypertension*. 2012;59:1195–1203.
32. Kassiri Z, Oudit GY, Sanchez O, Dawood F, Mohammed FF, Nuttall RK, Edwards DR, Liu PP, Backx PH, Khokha R. Combination of tumor necrosis factor-alpha ablation and matrix metalloproteinase inhibition prevents heart failure after pressure overload in tissue inhibitor of metalloproteinase-3 knock-out mice. *Circ Res*. 2005;97:380–390.
33. Wright CD, Chen Q, Baye NL, Huang Y, Healy CL, Kasinathan S, O'Connell TD. Nuclear alpha1-adrenergic receptors signal activated ERK localization to caveolae in adult cardiac myocytes. *Circ Res*. 2008;103:992–1000.
34. Sutton MG, Sharpe N. Left ventricular remodeling after myocardial infarction: pathophysiology and therapy. *Circulation*. 2000;101:2981–2988.
35. Japp AG, Cruden NL, Amer DA, Li VK, Goudie EB, Johnston NR, Sharma S, Neilson I, Webb DJ, Megson IL, Flapan AD, Newby DE. Vascular effects of apelin in vivo in man. *J Am Coll Cardiol*. 2008;52:908–913.
36. Murza A, Parent A, Besserer-Offroy E, Tremblay H, Karadereye F, Beaudet N, Leduc R, Sarret P, Marsault E. Elucidation of the structure-activity relationships of apelin: influence of unnatural amino acids on binding, signaling, and plasma stability. *ChemMedChem*. 2012;7:318–325.
37. Yellon DM, Hausenloy DJ. Myocardial reperfusion injury. *N Engl J Med*. 2007;357:1121–1135.
38. Ware JA, Simons M. Angiogenesis in ischemic heart disease. *Nat Med*. 1997;3:158–164.
39. Carmeliet P. Angiogenesis in life, disease and medicine. *Nature*. 2005;438:932–936.
40. Liu S, Premont RT, Kontos CD, Huang J, Rockey DC. Endothelin-1 activates endothelial cell nitric-oxide synthase via heterotrimeric G-protein betagamma subunit signaling to protein jinase B/Akt. *J Biol Chem*. 2003;278:49929–49935.
41. Ridgway J, Zhang G, Wu Y, Stawicki S, Liang WC, Chanthery Y, Kowalski J, Watts RJ, Callahan C, Kasman I, Singh M, Chien M, Tan C, Hongo JA, de Sauvage F, Plowman G, Yan M. Inhibition of Dll4 signalling inhibits tumour growth by deregulating angiogenesis. *Nature*. 2006;444:1083–1087.
42. del Toro R, Prahst C, Mathivet T, Siegfried G, Kaminker JS, Larrivee B, Breant C, Duarte A, Takakura N, Fukamizu A, Penninger J, Eichmann A. Identification and functional analysis of endothelial tip cell-enriched genes. *Blood*. 2010;116:4025–4033.
43. Oudit GY, Penninger JM. Cardiac regulation by phosphoinositide 3-kinases and PTEN. *Cardiovasc Res*. 2009;82:250–260.
44. Heineke J, Molkentin JD. Regulation of cardiac hypertrophy by intracellular signalling pathways. *Nat Rev Mol Cell Biol*. 2006;7:589–600.
45. Medhurst AD, Jennings CA, Robbins MJ, Davis RP, Ellis C, Winborn KY, Lawrie KW, Hervieu G, Riley G, Bolaky JE, Herrity NC, Murdock P, Darker JG. Pharmacological and immunohistochemical characterization of the APJ receptor and its endogenous ligand apelin. *J Neurochem*. 2003;84:1162–1172.
46. Ishida J, Hashimoto T, Hashimoto Y, Nishiwaki S, Iguchi T, Harada S, Sugaya T, Matsuzaki H, Yamamoto R, Shiota N, Okunishi H, Kihara M, Umemura S, Sugiyama F, Yagami K, Kasuya Y, Mochizuki N, Fukamizu A. Regulatory roles for APJ, a seven-transmembrane receptor related to angiotensin-type 1 receptor in blood pressure in vivo. *J Biol Chem*. 2004;279:26274–26279.
47. Condorelli G, Drusco A, Stassi G, Bellacosa A, Roncarati R, Iaccarino G, Russo MA, Gu Y, Dalton N, Chung C, Latronico MV, Napoli C, Sadoshima J, Croce CM, Ross J Jr. Akt induces enhanced myocardial contractility and cell size in vivo in transgenic mice. *Proc Natl Acad Sci USA*. 2002;99:12333–12338.
48. Sartoretto JL, Kalwa H, Pluth MD, Lippard SJ, Michel T. Hydrogen peroxide differentially modulates cardiac myocyte nitric oxide synthesis. *Proc Natl Acad Sci USA*. 2011;108:15792–15797.
49. Iwanaga Y, Kihara Y, Takenaka H, Kita T. Down-regulation of cardiac apelin system in hypertrophied and failing hearts: possible role of angiotensin II-angiotensin type 1 receptor system. *J Mol Cell Cardiol*. 2006;41:798–806.
50. D'Aniello C, Lonardo E, Iaconis S, Guardiola O, Liguoro AM, Liguori GL, Autiero M, Carmeliet P, Minchiotti G. G protein-coupled receptor APJ and its ligand apelin act downstream of Cripto to specify embryonic stem cells toward the cardiac lineage through extracellular signal-regulated kinase/p70S6 kinase signaling pathway. *Circ Res*. 2009;105:231–238.
51. Wang IN, Wang X, Ge X, Anderson J, Ho M, Ashley E, Liu J, Butte MJ, Yazawa M, Dolmetsch RE, Quertermous T, Yang PC. Apelin enhances directed cardiac differentiation of mouse and human embryonic stem cells. *PLoS ONE*. 2012;7:e38328.
52. Walsh K, Shiojima I. Cardiac growth and angiogenesis coordinated by intertissue interactions. *J Clin Invest*. 2007;117:3176–3179.
53. Alastalo TP, Li M, Perez Vde J, Pham D, Sawada H, Wang JK, Koskenvuo M, Wang L, Freeman BA, Chang HY, Rabinovitch M. Disruption of PPARgamma/beta-catenin-mediated regulation of apelin impairs BMP-induced mouse and human pulmonary arterial EC survival. *J Clin Invest*. 2011;121:3735–3746.
54. Iturrioz X, Alvear-Perez R, De Mota N, Franchet C, Guillier F, Leroux V, Dabire H, Le Jouan M, Chabane H, Gerbier R, Bonnet D, Berdeaux A, Maigret B, Galzi JL, Hibert M, Llorens-Cortes C. Identification and pharmacological properties of E339-3D6, the first nonpeptidic apelin receptor agonist. *FASEB J*. 2010;24:1506–1517.